UNCLASSIFIED

SECURITY CLASSIFICATION OF THIS PAGE (When Data Entered)

LEVEL III

REPORT DOCUMENTATION PAGE

READ INSTRUCTIONS BEFORE COMPLETING FORM

1. REPORT NUMBER	2. GOVT ACCESSION NO. AD-A089 006
3. RECIPIENT'S CATALOG NUMBER	
4. TITLE (and Subtitle) (6) Application of Solidification Theory to Rapid Solidification Processing	5. TYPE OF REPORT & PERIOD COVERED Semi-Annual Tech Rpt.
	6. PERFORMING ORG. REPORT NUMBER
7. AUTHOR(s) National Bureau of Standards Center for Materials Science Wash., DC 20235	8. CONTRACT OR GRANT NUMBER(s) AO 3751 (15) ARPA Order-3751
9. PERFORMING ORGANIZATION NAME AND ADDRESS DARPA 1400 Wilson Blvd. Arlington, VA 22209 (10) W.J. Boettinger J.W. Cahn S.R. Coriell J.R. Manning	10. PROGRAM ELEMENT, PROJECT, TASK AREA & WORK UNIT NUMBERS 9D10
11. CONTROLLING OFFICE NAME AND ADDRESS (11)	12. REPORT DATE May 1980
	13. NUMBER OF PAGES 54 (12) 59
14. MONITORING AGENCY NAME & ADDRESS (if different from Controlling Office) Semi-Annual technical rept. 1 Oct 79 - 31 Mar 80,	15. SECURITY CLASS. (of this report) Unclassified
	15a. DECLASSIFICATION/DOWNGRADING SCHEDULE NA

16. DISTRIBUTION STATEMENT (of this Report)

APPROVED FOR PUBLIC RELEASE - DISTRIBUTION UNLIMITED

17. DISTRIBUTION STATEMENT (of the abstract entered in Block 20, if different from Report)

NA

DTIC ELECTE SEP 11 1980 S D E

18. SUPPLEMENTARY NOTES

NA

THIS DOCUMENT IS BEST QUALITY PRACTICABLE. THE COPY FURNISHED TO DDC CONTAINED A SIGNIFICANT NUMBER OF PAGES WHICH DO NOT REPRODUCE LEGIBLY.

19. KEY WORDS (Continue on reverse side if necessary and identify by block number)

Materials
Metallurgy
Solidification Processing
Metallic Glasses

20. ABSTRACT (Continue on reverse side if necessary and identify by block number)

This semi-annual technical report for ARPA Order 3751 covers the period 1 Oct 79 to 31 Mar 80. Work is reported in the following areas of rapid solidification processing: (1) Interface Stability during Rapid Solidification, (2) Eutectic Solidification and the Formation of Metallic Glasses, and (3) Thermodynamics of Metastable Equilibria.

387444 JOB

DD FORM 1 JAN 73 1473 EDITION OF 1 NOV 65 IS OBSOLETE

Unclassified

SECURITY CLASSIFICATION OF THIS PAGE (When Data Entered)

AD A089006

DDC FILE COPY

DISCLAIMER NOTICE

THIS DOCUMENT IS BEST QUALITY PRACTICABLE. THE COPY FURNISHED TO DTIC CONTAINED A SIGNIFICANT NUMBER OF PAGES WHICH DO NOT REPRODUCE LEGIBLY.

Application of Solidification Theory to Rapid Solidification Processing

W. J. Boettinger, J. W. Cahn, S. R. Coriell and J. R. Manning
Metallurgy Division
Center for Materials Science
National Bureau of Standards
Washington, D. C. 20234

Semi-Annual Technical Report
Period Covered: October 1, 1979 to March 31, 1980
ARPA Order No. 3751

Report Issued: May 1980

Prepared for
Defense Advanced Research Projects Agency
Arlington, Virginia 22209

Program Code No: 9D10
Effective Date of Contract: April 1, 1979
Contract Expiration Date: March 31, 1982
Principal Investigator: J. R. Manning
(301) 921-3354

Table of Contents

Application of Solidification Theory to Rapid Solidification Processing

1. Technical Report Summary

This semi-annual technical report for ARPA Order 3751 covers the period October 1, 1979 to March 31, 1980. Work is reported in the following areas of rapid solidification processing: (1) Interface Stability during Rapid Solidification, (2) Eutectic Solidification and the Formation of Metallic Glasses, and (3) Thermodynamics of Metastable Equilibria. Manuscripts have been prepared for publication in each of these areas and will be published in the Proceedings of the Second International Conference on Rapid Solidification Processing: Principles and Technologies. This conference was held March 24-26, 1980 in Reston, Va. These papers are included here as the main body of this semi-annual report. In addition, a paper entitled Rapid Solidification, which reviews earlier work here, is included as a final item in this report. This paper was presented at the conference on Laser and Electron Beam Processing of Materials held November 1979 in Boston, Massachusetts, and will be published in the proceedings of that meeting.

Task Objective

The objective of this work is to investigate the theory of rapid solidification to determine whether major aspects of rapid solidification processes can be explained by conventional solidification theory and to examine non-equilibrium effects which can arise. In particular, segregation effects, glass-forming tendencies, and rules governing the formation of equilibrium and non-equilibrium phases, including alloy composition limits, reaction sequences and metastable phase formation, will be investigated.

Technical Problem and General Methodology

During the freezing of alloys, a planar solid-liquid interface can become unstable; this leads to a cellular or dendritic interface and causes solute microsegregation. The transition between planar and non-planar growth during the directional solidification of binary alloys is being investigated using morphological stability theory. Conventional constitutional supercooling theory predicts that the stability of planar solidification interfaces will decrease as solidification velocities increase. At large solidification velocities, however, morphological stability considerations predict that planar interface stability will increase with solidification velocity. Calculations are being done for rapid solidification conditions to determine the effect of solidification velocity on interface stability.

Eutectic alloy compositions are frequently found to provide favorable conditions for formation of metallic glasses. The theory of how rapidly one needs to solidify to obtain a glassy structure has usually focussed on the nucleation of the solid phase as the difficult step in crystallization. In the present work, the focus instead is on the growth process. Diffusional sorting of alloy components is necessary to form a two-phase eutectic composite structure. Theoretical predictions can be made of the limitation this imposes on eutectic spacing and at sufficiently rapid solidification rates this diffusional sorting would no longer be possible, perhaps resulting in amorphous solids being formed. Experimental methods designed to solidify eutectic alloys at known velocities and temperature gradients and to test this theory by providing quantitative correlation of alloy microstructure, such as eutectic spacing or glass formation, with solidification conditions are being developed. Two methods are being pursued: (1) rapid directional

solidification at controlled speeds up to 10 cm/s and (2) electron beam surface melting for solidification at higher velocities.

Rapid solidification processes are frequently regarded as leading to non-equilibrium conditions which cannot be predicted by theories restricted to conventional equilibrium thermodynamics. Nevertheless, a careful consideration of thermodynamic phase reactions and limits on metastable phases may adequately describe a number of rapid solidification effects. The thermodynamic theory of multiphase systems is being investigated to determine rules that should control metastable reaction sequences, relative stability of heterogeneous microstructure and compositional limits imposed by the thermodynamics during rapid solidification.

Technical Results, Important Findings and Conclusions

Detailed methods and results are described in the main body of the report. Important new results, findings and conclusions include:

(a) The phenomenon of solid-liquid interface stability during directional solidification of a binary alloy was reexamined with special emphasis on very rapid solidification rates. Although at low to moderate solidification rates an increase in solidification velocity leads to a decrease in interface stability, it was found at very rapid solidification rates (above 0.01 m/s in copper containing aluminum), the perturbation theory predicts a strong increase in stabilization. There appear to be two dominant effects leading to this result. The first effect, known as absolute stability can occur even if there is local equilibrium at the solid-liquid interface. This effect arises because only short wavelength perturbations are important at high velocities and these are stabilized by surface energy. Numerical calculations for aluminum with various concentrations of copper and a liquid temperature

gradient of $2(10^4)$ K/m show that absolute stability is important for solidification velocities above about 0.01 m/s; in fact, for copper concentrations less than $6x10^{-3}$ wt. %, the interface is stable at any solidification rate. The second effect is caused by departure from local equilibrium at the solid-liquid interface. Although the exact forms of such departures, let alone their magnitude, is not well known, the perturbation theory can be modified to include their salient features. Most departures from local equilibrium lead to increased stability. For example, all constitutional effects will vanish as the distribution coefficient approaches unity.

(b) The relationship between eutectic solidification and the ease of formation of metallic glasses is being investigated. For many systems, crystallization, including partitionless crystallization, of alloys into a single phase solid is impossible over a wide range of composition near stable or metastable eutectics. This fact forces alloys to crystallize into two-phase solids. Because of the need for diffusional sorting of the components and creation of solid-solid surfaces, the kinetics of eutectic crystallization are relatively slow and may be closely related to the ease of glass formation of these alloys.

Experiments were done on the directional solidification of Pd-6 at % Cu-17 at % Si alloys which show the evolution of microstructure as a function of interface velocity. A structure of dendrites and interdendritic eutectic at low velocity ($\lesssim$ 0.25 mm/s) becomes a fine eutectic-like structure at intermediate velocities ($\sim$ 1 mm/s) and finally the alloy forms glass when crystallization is attempted at velocities greater than 2.5 mm/s.

(c) The thermodynamics of metastable phase equilibrium can be shown to be closely related to that of stable phase equilibrium. Metastable phase

equilibrium often can be represented by extensions of the curves on phase diagrams that represent stable phase equilibria. Thermodynamic principles rank phase equilibria but not phases in a hierarchy of increasing stability. Thermodynamics imposes precursor rules in multicomponent systems in which a prior reaction is required before a phase can appear. A given hierarchy persists over a domain on the phase diagram bounded by surfaces on which the ranking of two equilibria changes. Multicomponent phases per se do not form a hierarchy because a given phase can disappear and reappear in a sequence of spontaneous processes. Processing for producing metastable phases must place the system within a domain in which the desired phases can form spontaneously from the available phases.

(d) Modifications were made to an electron beam melting apparatus at NBS to allow improved surface melting experiments to be performed.

Special Comments

NBS personnel from this contract played major roles in organizing the Second International Conference on Rapid Solidification Processing held March 24-26, 1980 in Reston, Va. Attendance at the conference was more than 170. The Chairman of the Conference Steering Committee was Robert Mehrabian, Chief of the NBS Metallurgy Division and the Conference Secretary-Treasurer was John Manning. This conference was co-sponsored by DARPA, ONR, AFML, ARO and NBS. A conference proceedings, containing more than 40 papers, will be published. Robert Mehrabian is Chairman of the Conference Publications Committee. Three of the papers written for this proceedings by NBS authors, which report work done on the current contract, are included as part of this semi-annual report.

During the period covered by this semi-annual report, Dr. R. Schaefer, formerly of the Naval Research Laboratory, joined our staff and has begun work on electron beam melting aspects of this work. Prof. T. Massalski of Carnegie-Mellon University also is at NBS in the Metallurgy Division this year and is contributing as a consultant to the current work.

Plans and Implications for Future Research

Since the current work has shown that glass formation can be obtained during directional solidification of Cu-Si-Pd alloys, this system will be studied in more detail to permit a semi-quantitative evaluation of equations concerning the effect of solidification velocities. Future work will include attempts to measure interface temperature, temperature gradient, and the eutectic spacing along with an identification of phases present during eutectic solidification at velocities just below the transition to the glass. Additionally, experiments on the electron beam melting of Al-Ag and Al-Cu alloys will be initiated to test morphological stability theory at high velocity and to determine the critical conditions for the onset of massive (partitionless) solidification, respectively.

Future work on theoretical aspects of this problem will include investigation of solute segregation due to curved solid-liquid interfaces, the effect of non-constant velocities on interface stability during rapid solidification, and further calculations of interface stability during growth into supercooled liquids. Equations will be developed to bring into morphological stability theory the crystal anisotropies and apply the results to high solidification velocities. The tendency that cells may have to follow the heat flow direction rather than to take on crystallographic forms characteristic of ordinary cells and dendrites will be investigated.

2. Report of Technical Progress and Results

Four manuscripts were prepared for publication during the period covered by this semi-annual report. Since these papers present the major results obtained in work on this contract they are included here as the report on technical progress and results. The papers on "Interface Stability During Rapid Solidification," "Eutectic Solidification and Formation of Metallic Glasses," and "Thermodynamics of Metastable Equilibria" will be published in the Proceedings of the Second International Conference on Rapid Solidification Processing, held March 1980 in Reston, Virginia. The paper on " Rapid Solidification" will be published in Laser and Electron Beam Processing of Materials, edited by C. W. White and P. S. Peercy, Materials Research Society (proceedings of conference held Nov. 1979 in Boston, Massachusetts).

Interface Stability During Rapid Solidification

S. R. Coriell

National Bureau of Standards
Washington, DC 20234

and

R. F. Sekerka*

Carnegie-Mellon University
Pittsburgh, PA 15213

ABSTRACT

The phenomenon of solid-liquid interface stability during directional solidification of a binary alloy is reexamined with special emphasis on very rapid solidification rates. For ordinary solidification rates, the predictions of the perturbation theory of morphological stability lead to results that are similar to those implied by constitutional supercooling; however, at very rapid solidification rates, the perturbation theory predicts a vast increase in stabilization in comparison to constitutional supercooling. There appear to be two dominant effects. The first effect can occur even if there is local equilibrium at the solid-liquid interface; it is known as absolute stability and arises because only short wavelength perturbations are important at high velocities and these are stabilized by surface energy. Numerical calculations for aluminum with various concentrations of copper and a liquid temperature gradient of $2(10^4)$ K/m show that absolute stability is important for solidification velocities above about 0.01 m/s; in fact, for copper concentrations less than 6×10^{-3} wt. %, the interface is stable at any solidification rate. The second effect is caused by departure from local equilibrium at the solid-liquid interface. Although the exact forms of such departures, let alone their magnitude, is not well known, the perturbation theory can be modified to include their salient features. Most departures from local equilibrium lead to increased stability. For example, all constitutional effects will vanish as the distribution coefficient approaches unity. Finally, other factors are examined with an aim toward the identification of a realm where experimental test of the theory would be meaningful.

* Consultant, National Bureau of Standards

I. Introduction

For about the last thirty years, the principle of constitutional supercooling[1] has been used as a guideline to ascertain the growth conditions that result in solid-liquid interface shape instability during alloy solidification. For about the last twenty of those thirty years, this principle has been complemented and extended by the theory of morphological stability.[2-4] The approaches of these analyses are somewhat different, constitutional supercooling being largely an application of thermodynamics to decide if a liquid is supercooled (and therefore deemed to be unstable) with due respect to its composition, and morphological stability theory being a detailed kinetic analysis of the growth or decay of a perturbation according to the laws of heat flow and diffusion. Extensive reviews are available in the literature.[5-9]

Despite the different approaches of the constitutional supercooling principle and morphological stability theory, there are a large number of common situations where they lead to similar results, or at least similar trends within the inaccuracies of our knowledge of system and material parameters. For this reason, the constitutional supercooling principle is widely used because of its simplicity. Nevertheless, there are situations where these two approaches can lead to quite different results. One such situation occurs when the average temperature gradient (namely $(k_s G_s + k_L G_L)/(k_s + k_L)$, where G_s and G_L are temperature gradients in solid and liquid, respectively, and k_s and k_L are the corresponding thermal conductivities) is significantly different from G_L, the only temperature gradient that the constitutional supercooling principle considers. A second more dramatic situation occurs in the case of melting, as analysed by [illegible]n and Jackson,[10] for which constitutional superheating underestimates stability by orders of magnitude because it uses the diffusivity of the solid rather than the diffusivity of the liquid (where the relevant solute transport occurs).

A third situation where constitutional supercooling and morphological stability lead to quite different answers - indeed, the main subject of the present paper - is the case of rapid solidification. At very rapid rates of solidification, the perturbation theory predicts a vast increase in stabilization in comparison to constitutional supercooling. There appear to be two dominant effects. The first effect can occur even if there is local equilibrium at the solid-liquid interface; it is known as absolute stability[3] and arises because only short wavelength perturbations are important at high velocities and these are stabilized by surface energy. This case will be presented in Section II and illustrated with specific application to dilute alloys of Cu in Al. The second effect is caused by departure from local equilibrium at the

solid-liquid interface and is taken up in Section III. Section IV is devoted to the special case of a supercooled liquid and the results applied to the solidification of small droplets.

We emphasize that the analyses of the present paper deal with constant solidification rates and initially planar interfaces. The case of non-constant high solidification rates - although typical of many experimental situations - has only been tractable in special cases.[11]

II. Local Equilibrium and the Transition to Absolute Stability

We consider the morphological stability of a planar solid-liquid interface during unidirectional solidification of a binary alloy at constant velocity V. We outline a standard[12] linear time dependent stability analysis and then focus our attention to large velocities where absolute stability prevails and our results differ significantly from those of constitutional supercooling.

We choose an (x,y,z) coordinate system (moving with the planar interface) such that the solid-liquid interface is described by $z = W(x,y,t)$ where t is the time. We assume that $W(x,y,t)$ and any of its derivatives are sufficiently small that any nonlinear terms can be neglected.

We solve the differential equations

$$(\partial T_L/\partial t) = \kappa_L \nabla^2 T_L + V(\partial T_L/\partial z), \tag{1a}$$

$$(\partial T_s/\partial t) = \kappa_s \nabla^2 T_s + V(\partial T_s/\partial z), \tag{1b}$$

$$(\partial c/\partial t) = D\nabla^2 c + V(\partial c/\partial z), \tag{1c}$$

where T_L and T_s are temperatures in the liquid and solid, respectively, c is the concentration of solute in the liquid (diffusion in the solid is neglected), κ_L and κ_s are thermal diffusivities of liquid and solid, respectively, and D is the diffusion coefficient of solute in the liquid.

The boundary conditions far from the solid-liquid interface are

$$(\partial T_L/\partial z) = G_L \exp(-Vz/\kappa_L) \qquad z \to \infty, \tag{2a}$$

$$(\partial T_s/\partial z) = G_s \exp(-Vz/\kappa_s) \qquad z \to -\infty, \tag{2b}$$

$$c = c_\infty \qquad z \to \infty, \tag{2c}$$

where the temperature gradients G_L and G_s and the solute concentration c_∞ are constants. We consider $G_s \geq 0$ and $G_L \geq 0$; the case $G_L < 0$ will be discussed in Section IV.

The boundary conditions at the solid-liquid interface are

$$T_L = T_s \tag{3a}$$

$$v = V + (\partial W/\partial t) \tag{3b}$$

$$v = (k_s/L_v)(\partial T_s/\partial z) - (k_L/L_v)(\partial T_L/\partial z) \tag{3c}$$

$$v = - D(\partial c/\partial z)/(c-c_s) \tag{3d}$$

$$T_L = T_e \equiv T_M - T_M\Gamma K + g(c) \tag{3e}$$

$$c_s = h_0(c), \tag{3f}$$

where v is the interface velocity, k_s and k_L are thermal conductivities of solid and liquid, respectively, L_v is the latent heat per unit volume, c_s is the concentration in the solid at the interface, T_M is the melting point of a flat interface in the absence of solute, Γ is the ratio of the solid-liquid surface tension γ to the latent heat per unit volume, $K = - (\partial^2 W/\partial x^2) - (\partial^2 W/\partial y^2)$ is the interface curvature, the dependence of melting point on solute is given by the function g(c) and the relationship between c_s and c is given by the function $h_o(c)$. Equations (3e) and (3f) are based on the assumption of local equilibrium at the solid-liquid interface. In Equation (3c) we have ommitted corrections[13] that might arise from consideration of surface entropy and also a possible dependence of g(c) and $h_0(c)$ on curvature.[3]

In carrying out a linear stability analysis, we write the temperature and concentration fields as a sum of an unperturbed part, which is a function of z alone, and a perturbed part which is of the form $F_j(z) \exp [\sigma t + i(\omega_x x + \omega_y y)]$, where F_j is a function of z alone. The perturbed solid-liquid interface is given by

$$z = W(x,y,t) = \delta \exp [\sigma t + i(\omega_x x + \omega_y y)], \tag{4}$$

where δ is the perturbation amplitude at $t = 0$, and ω_x and ω_y are spatial frequencies. The interface is unstable if the real part of the time constant σ is positive for any perturbation, i.e., any real values of ω_x and ω_y. The interface is stable if the real part of σ is negative for all perturbations.

Upon solving the differential equations, one finds

$$\sigma = V\{-k_L G_L(\alpha_L - V/\kappa_L) - k_s G_s(\alpha_s + V/\kappa_s) - 2\bar{k}T_M\Gamma\omega^2\bar{\alpha} + 2\bar{k}mG_c\bar{\alpha}(\alpha - V/D)/(\alpha - pV/D)\}/\{L_v V + 2\bar{k}mC_c\bar{\alpha}/(\alpha - pV/D)\} \quad (5)$$

with

$$\alpha = (V/2D) + [(V/2D)^2 + \omega^2 + \sigma/D]^{\frac{1}{2}},$$

$$\alpha_L = (V/2\kappa_L) + [(V/2\kappa_L)^2 + \omega^2 + \sigma/\kappa_L]^{\frac{1}{2}}$$

$$\alpha_s = -(V/2\kappa_s) + [(V/2\kappa_s)^2 + \omega^2 + \sigma/\kappa_s]^{\frac{1}{2}}$$

$$\bar{\alpha} = (k_s\alpha_s + k_L\alpha_L)/(2\bar{k}),$$

where $2\bar{k} = k_s + k_L$, $\omega^2 = \omega_x^2 + \omega_y^2$, $G_c = Vc_0(k-1)/D$, $k = c_\infty/c_0$, $m = (dg/dc)$ and $p = 1 - (dh_0/dc)$ with the derivatives evaluated at $c = c_0$ and c_0 defined by the equation $c_\infty = h_0(c_0)$, i.e., c_0 is the solute concentration in the liquid at the planar solid-liquid interface. If one assumes that the functions $g(c)$ and $h_0(c)$ are linear in c, then m, k, and $p = 1 - k$ are constants independent of c.

For a given alloy and processing conditions, we can calculate $\sigma(\omega)$ from equation (5). If the real part of σ is positive for any value of ω, the interface is unstable. Alternately we can specify the real part of σ, σ_r, and calculate some other variable such as c_∞ as a function of ω. For $\sigma_r = 0$, the minimum value of $c_\infty(\omega)$, which occurs at some specific value of ω, gives the stability-instability demarcation. Except where otherwise specified, we have also assumed that the imaginary part of σ, σ_i, is zero at the stability-instability demarcation, consistent with a detailed analysis in the thermal steady state approximation.[12]

We have carried out numerical calculations for alloys of aluminum containing copper for the following values of material parameters:

$$k_L = 90.7\text{J/(msK)}, \quad k_s = 210\text{J/(msK)},$$

$$L_v = 1.08\text{GJ/m}^3, \quad T_M\Gamma = 1.0(10^{-7})\text{mK},$$

$$\kappa_L = 4.2(10^{-5})\text{m}^2/\text{s}, \quad \kappa_s = 8.1(10^{-5})\text{m}^2/\text{s},$$

$$D = 5(10^{-9})\text{m}^2/\text{s}, \quad k = 0.14, \quad m = -2.5\ \text{K/(wt. \%)}.$$

The curve in Fig. 1, based on equation (5), shows the critical copper concentration (below which the planar interface is stable) as a function of growth velocity V for a temperature gradient in the liquid, G_L, of $2(10^4)$ K/m. The dashed straight line with negative slope is the constitutional supercooling criterion, $mG_c = G_L$, and the straight line with positive slope is the absolute stability criterion, $mG_c = kT_M\Gamma(V/D)^2$ (see eq. (7) et seq.). The constitutional supercooling criterion is a good approximation at low velocities and the absolute stability criterion is a good approximation at high velocities. In Fig. 2, the wavelength $\lambda = 2\pi/\omega$ that corresponds to the onset of instability, i.e. to the value of ω for which $c_\infty(\omega)$ is a minimum, is shown to be a monotonically decreasing function of interface velocity. Although results are given in Figs. 1 and 2 for V = 10 m/s, the theory should not be taken seriously at these velocities since the diffusion length D/V is of atomic dimensions.

From Fig. 2, one finds that $(V/2\kappa_s) \ll \omega$ and $(V/2\kappa_L) \ll \omega$, which permits the use of the thermal steady state approximation according to which we let the thermal diffusivities approach infinity. For the stability-instability demarcation ($\sigma = 0$), Equation (5) then reduces to

$$0 = V\omega\{-k_L G_L - k_s G_s - 2\bar{k}T_M\Gamma\omega^2 + 2\bar{k}mG_c(\alpha - V/D)/(\alpha - pV/D)\}/$$

$$\{L_v V + 2\bar{k}mG_c\omega/(\alpha - pV/D)\}. \qquad (6)$$

The denominator is always positive so that only the properties of the numerator need be analyzed. The stability criterion may be written as[14]

$$2k_L G_L + VL_v > 2\bar{k}mG_c S(A,k), \qquad (7)$$

where S is a function of the dimensionless variables k and $A = kT_M\Gamma V^2/(D^2 mG_c)$. For $A \geq 1$, the interface is always stable, while for $A < 1$, the spatial frequency ω_m at the onset of instability and the function S(A,k), which lies between zero and unity, can be calculated by finding the one and only real positive root of the cubic equation

$$r^3 + (2k-1)\,r - (2k/A^{1/2}) = 0. \qquad (8)$$

The quantities S and ω_m are then given by

$$S(A,k) = 1 + (A/4k)(1 - r^2 + 2k\cdot^{\cdot}) - (3A^{1/2}r/2), \qquad (9)$$

$$\omega_m = (V/2D)(r^4 - 1)^{1/2}. \qquad (10)$$

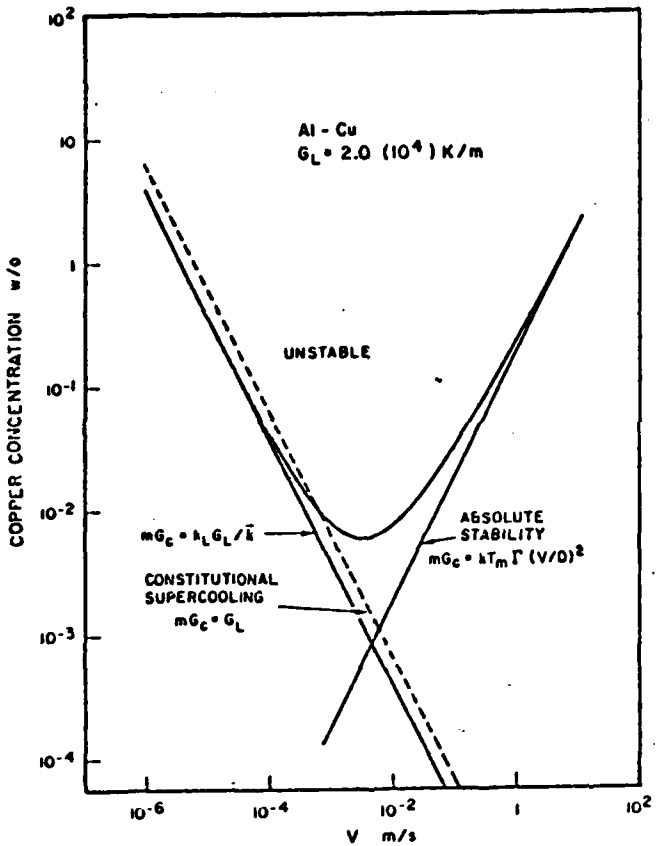

Figure 1. The critical concentration of copper above which interface instability occurs as a function of the interface velocity V of directional solidification of aluminum for a temperature gradient in the liquid of 2.0(10^4)K/m. The curve is based on morphological stability theory while the lines correspond to constitutional supercooling, modified constitutional supercooling, and absolute stability.

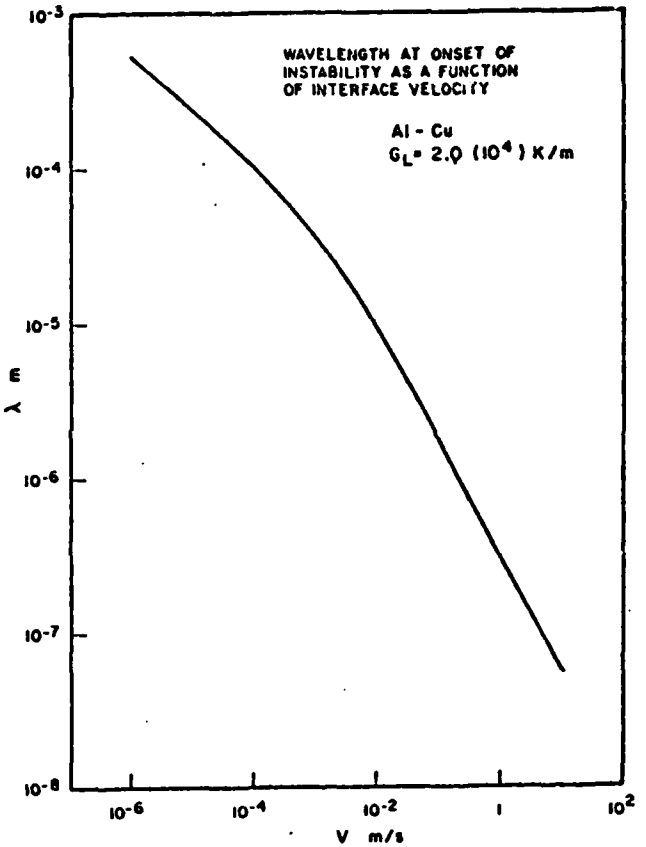

Figure 2. The wavelength λ at the onset of instability during directional solidification of aluminum containing copper as a function of interface velocity V.

Rewriting equation (10) in the form $r^4 = 1 + (2D\omega_m/V)^2$, we recognize two limiting cases, viz., $(2D\omega_m/V) >> 1$ and $(2D\omega_m/V) << 1$. First, we consider $(2D\omega_m/V) >> 1$, and consequently $r >> 1$. The solution of equation (8) is then $r^3 = 2k/A^{\frac{1}{2}}$. It follows that $S = 1 - (3k/r^2)$ and $\omega_m = (V/2D)r^2 = [(kV/4\bar{k}T_M\Gamma D)(2k_LG_L + VL_v)]^{1/3}$. If, in addition, $VL_v << 2k_LG_L$, then $\omega_m = [kk_LG_LV/2\bar{k}T_M\Gamma D]^{1/3}$, and the stability criterion is $(k_L/\bar{k})G_L = mC_c$, which is shown as the solid line with negative slope in Fig. 1. At low velocities this line is a better approximation to the curve than constitutional supercooling to which it would be identical for $k_s = k_L$. The proportionality[15] between ω_m and $V^{1/3}$ is in agreement with the experimental data of Morris and Winegard[16] on lead-antimony alloys.

For the second limiting case, $(2D\omega_m/V) << 1$ and $r \to 1$. If we let $r = 1 + \varepsilon$ with $0 < \varepsilon << 1$, then

$$\varepsilon = [k/(1+k)][(1-A^{\frac{1}{2}})/A^{\frac{1}{2}}],$$

$$S = [(1-k/2)/(1+k)](1-A^{\frac{1}{2}})^2,$$

$$\omega_m = \{[kV^2(VL_v+2k_LG_L)]/[(1+k)(1-k/2)2\bar{k}T_M\Gamma D^2]\}^{\frac{1}{4}},$$

and the stability criterion approaches the absolute stability criterion $A = 1$. For $VL_v >> 2kG_L$, we have

$$\omega_m = \{[kV^3L_v]/[(1+k)(1-k/2)2\bar{k}T_M\Gamma D^2]\}^{\frac{1}{4}}$$

Thus for small velocities $(2D\omega_m/V) >> 1$ and ω_m is proportional to $V^{1/3}$ while for large velocities $(2D\omega_m/V) << 1$ and ω_m is proportional to $V^{3/4}$. These approximations are verified by the results in Fig. 2. Plots of $S(A,k)$ and additional analytic results are available.[14]

We close this section with two additional numerical examples for Al-Cu alloys. The first of these illustrates the effect of G_L on the critical concentration for instability at a sufficiently large solidification velocity that constitutional supercooling is a poor approximation. From Figs. 1 and 2, at a velocity of 1 m/s the critical concentration is 0.21 wt. % Cu and $\omega_m = 2.05\ (10^7)m^{-1}$ for $G_L = 2(10^4)K/m$. Moreover equation (7) shows that the instability criterion will be practically independent of G_L provided that $G_L << VL_v/2k_L = 6(10^6)K/m$. Calculations for higher values, viz. $G_L = 10^6$, 10^7, $10^8K/m$, give critical concentrations of 0.22, 0.24, and 0.34 wt. % and $\omega_m = 2.1(10^7)$, $2.6(10^7)$, and $4.2(10^7)m^{-1}$, respectively, indicating a relative insensitivity to the liquid temperature gradient.

The second numerical example illustrates the degree to which an instability can develop if only a finite time is available before solidification is complete. For V = 1m/s, a 100 μm layer will solidify in a time $t_c = 10^{-4}$s. In order to observe an unstable interface, the instability should be greatly amplified in a fraction of this time, i.e., we require that $\sigma t >> 1$ [see eq. (4)]. Taking $t = 0.1t_c = 10^{-5}$s, we require $\sigma >> 10^5\ s^{-1}$. Calculations with $G_L = 2(10^4)$K/m and $\sigma = 10^6$ and $10^7\ s^{-1}$ yield critical concentrations of 0.23 and 0.36 wt. % and $\omega_m = 2.1(10^7)$ and $3.4(10^7)m^{-1}$, respectively. These concentrations are in an experimentally accessible range but the wavelengths involved (~0.2 μm) would necessitate electron microscopy.

III. Departure from Local Equilibrium

We now briefly discuss the effect of departures from local equilibrium at the solid-liquid interface upon interface stability. We generalize the local equilibrium boundary conditions, equations (3e) and (3f), to the form[17-19]

$$v = f(T_e - T_I,\ c_I,\ T_I), \tag{3e'}$$

$$c_{sI} = h\ (c_I,\ T_e - T_I), \tag{3f'}$$

where the subscript I indicates evaluation at the solid-liquid interface. We require that $v = 0$ and $h = h_0$ when $T_e - T_I = 0$. We expand the above equations in a Taylor series about the temperature T_{I0}, equilibrium temperature T_{e0}, and solute concentration c_{I0} at the planar solid-liquid interface, viz.,

$$v = V + \mu_T[(T_e - T_{e0}) - (T_I - T_{I0})] + \mu_c(c_I - c_{I0}) + \mu_A(T_I - T_{I0}),$$

$$c_{sI} = h(c_{I0}, T_{c0} - T_{I0}) + k_c(c_I - c_{I0}) + k_T[(T_e - T_{e0}) - (T_I - T_{I0})],$$

where $\mu_T = \partial f/\partial(T_e - T_I)$, $\mu_c = \partial f/\partial c_I$, $\mu_A = \partial f/\partial T_I$, $k_c = \partial h/\partial c_I$, $k_T = \partial h/\partial(T_e - T_I)$ and the partial derivatives are evaluated at T_{e0}, T_{I0}, and c_{I0}. With this generalization, we obtain in place of equation (5)

$$\sigma = V\{[-k_L G_L(\alpha_L - V/\kappa_L) - k_s G_s(\alpha_s + V/\kappa_s)]U_A - 2\bar{k}T_M\Gamma\omega^2\bar{\alpha} -$$

$$+ 2\bar{k}m'C_c\bar{\alpha}(\alpha - V/D)/(\alpha - p'V/D)\}/[L_v V U_T$$

$$+ [2\bar{k}m'C_c\bar{\alpha}/(\alpha - p'V/D)]U_K\}, \tag{5'}$$

where $m' = m + (\mu_c/\mu_T)$, $p' = 1 - k_c + (k_T\mu_c/\mu_T)$,

$$U_A = 1 - [\mu_A/\mu_T][1 + (k_T m'V/D)/(\alpha - p'V/D)],$$

$$U_T = 1 - (\mu_A/\mu_T) + 2\bar{k}\,\bar{\alpha}/(L_v\mu_T),$$

and

$$U_K = 1 + [V^2 k_T/(\mu_T D G_c)][1 - L_v\mu_A/(2\bar{k}\,\bar{\alpha})].$$

As $\mu_T \to \infty$, we approach local equilibrium and equation (5′) approaches equation (5).

Although equation (5′) is rather general in allowing for deviations from local equilibrium, our knowledge concerning the forms of the functions f and h is extremely limited and quantitative conclusions based on equation (5′) are not possible. This is clearly an area in which experimental and theoretical research is desirable. We will attempt to draw some conclusions in a few simplified cases.

Case A $c_{sI} = c_I$

The deviation from equilibrium is so large that $k_c = 1$ and $G_c = 0$; there are no constitutional effects and the situation is similar to solidification of a pure material. In addition to there being no instability, there is no macrosegregation in contrast to the stable case for $k_c \neq 1$.

Case B $c_{sI} = h_0(c)$ and $v = f(T_e - T_I)$

Solid composition depends only on liquid composition as given by the phase diagram and velocity depends only on deviation of the temperature T_I from the temperature T_e. We have $\mu_c = \mu_A = k_T = 0$ so that $m' = m$, $p' = 1 - k_c$, $U_A = U_K = 1$, and $U_T = 1 + 2\bar{k}\,\bar{\alpha}/(L_v\mu_T)$. Thus, the numerator of equation (5′) is unchanged from the local equilibrium result, equation (5). Further, the denominator is still always positive since $\mu_T > 0$; the stability-instability demarcation is unaffected by μ_T. However, for sufficiently small μ_T we expect that σ will be reduced for fixed growth conditions or, alternatively, a larger value of concentration will be needed to obtain a given value of σ at fixed V. If

$$\mu_T >> [2\bar{k}\alpha V]/\{L_v V + 2\bar{k}mG_c\bar{\alpha}/[\alpha - pV/D]\} = D/(T_M\Gamma) = 0.05\text{m/sK}$$

holds (where the simplification to $D/T_M\Gamma$ is valid for large velocities), the term in the denominator involving μ_T is small compared to the sum of the other two terms, and μ_T has little effect. Since we are unaware of any reliable

measurements of μ_T for aluminum alloys, we have done some calculations for values of μ_T that bracket 0.05 m/sK. These calculations based on equation (5′) are summarized in Table 1; it follows that there is only a small increase in critical concentrations as μ_T decreases from ∞ to 0.1 m/sK but that critical concentrations nearly double as μ_T decreases from 0.1 to 0.01 m/sK Note that if f is a linear function of (T_e-T_I), then a velocity of 1 m/s and a kinetic coefficient μ_T of 0.01 m/sK correspond to a kinetic undercooling of 100K.

Case C pure material and $v = f(T_e-T_I, T_I)$

Temkin and Polyakov[19] have considered a kinetic law with the properties that $\mu_T > 0$ while $\mu_T - \mu_A > 0$ for T_I large (near T_M) and $\mu_T - \mu_A < 0$ for T_I sufficiently small. Such a kinetic law is sketched in Fig. 3 for two different values of equilibrium temperature, T_e' and T_e''. If one writes $v = F(T_e, T_I)$ instead of $v = f(T_e-T_I, T_I)$, then $\mu_T - \mu_A = -\partial F/\partial T_I$ and $\mu_T = \partial F/\partial T_e$, permitting geometrical interpretation via Fig. 3. A specific analytic example is $v = \mu_0(T_e-T_I) \exp(-\Theta/T_I)$, where μ_0 and Θ are constants, and from which $\mu_T = \mu_0 \exp(-\Theta/T_I)$ and $\mu_T - \mu_A = \mu_0 \exp(-\Theta/T_I)[1-\Theta(T_e-T_I)/T_I^2]$. For such a kinetic law, equation (5′) reduces to

$$\sigma = \{[-k_L G_L(\alpha_L - V/\kappa_L) - k_s G_s(\alpha_s + V/\kappa_s)][\mu_T - \mu_A] - \mu_T 2\bar{k} T_M \Gamma\omega^2 \bar{\alpha}\}/$$

$$\{L_v(\mu_T - \mu_A) + 2\bar{k}\,\bar{\alpha}\}. \qquad (11)$$

Note that $\mu_T - \mu_A = 0$ corresponds to the maximum in velocity as a function of T_I for fixed T_e.

So long as $\mu_T - \mu_A > 0$, analysis of equation (11) leads to results that are qualitatively similar to case B. If $\mu_T - \mu_A < 0$, further analysis is required since the sign of the denominator in equation (11) is not obvious. For simplicity, we let $k_s = k_L$ and $\kappa_s = \kappa_L$ so that $\bar{\alpha} = \{(V/2\kappa_L)^2 + \omega^2 + \sigma/\kappa_L\}^{\frac{1}{2}}$

TABLE I

CRITICAL CONCENTRATIONS AND SPATIAL FREQUENCIES FOR VARIOUS VALUES OF σ AND μ_T AT $G_L = 2(10^4)$K/m AND V = 1 m/s

$\sigma(s^{-1})$	μ_T(m/sK)	c_∞(wt. %)	$10^{-7}\omega_m(m^{-1})$
0	—	0.21	2.05
10^6	∞	0.23	2.1
10^7	∞	0.36	3.4
10^6	0.1	0.26	2.9
10^7	0.1	0.53	5.5
10^6	0.01	0.40	4.8
10^7	0.01	1.29	9.4

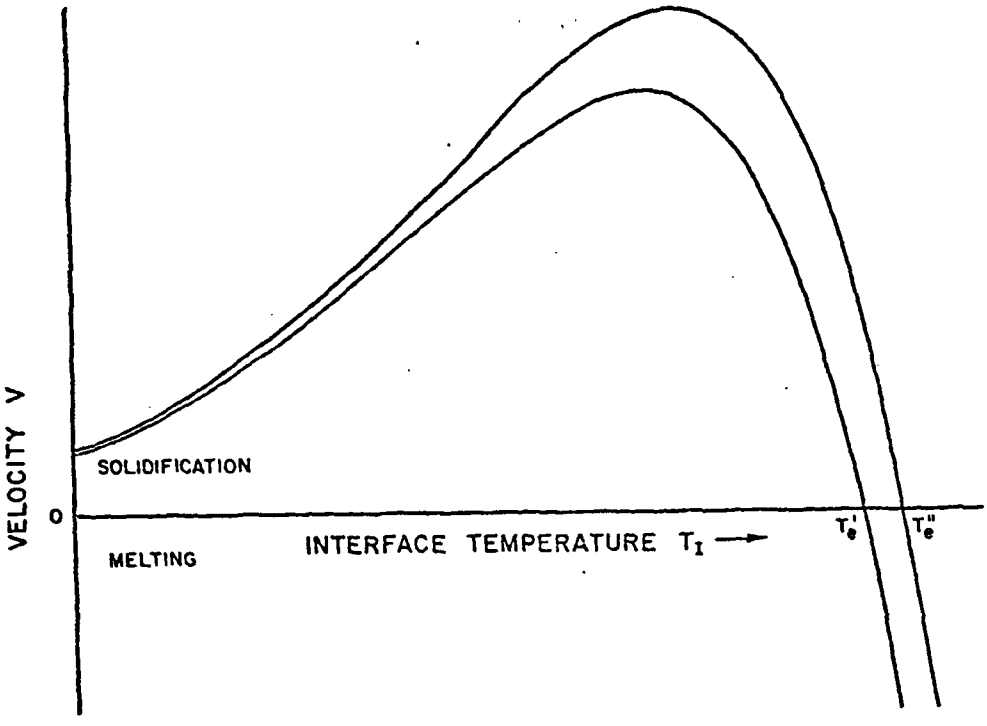

Figure 3. Sketch of interface velocity V as a function of interface temperature for two different values of the equilibrium temperature.

and

$$\sigma = \{[2k_s G_s \bar{\alpha} - VL_v(\bar{\alpha} - V/2\kappa_L)][\mu_A - \mu_T] - \mu_T 2k_L T_M \Gamma \omega^2 \bar{\alpha}\}/$$

$$\{2k_L \bar{\alpha} - L_v(\mu_A - \mu_T)\}. \qquad (12)$$

We consider growth into a supercooled liquid with $G_s = 0$. It is easy to show that $\sigma = 0$ is not a solution of equation (12) for any value of ω when $(\mu_T - \mu_A) < 0$. This suggests that we need to allow for the possibility that σ is complex. Numerical solution of equation (12) indicates that this is the case. Taking $\kappa_s = \kappa_L = 6.0(10^{-5})m^2/s$, $k_L = k_s = 150J/(msK)$, $\mu_T = 0.01m/sK$, $\mu_T - \mu_A = -0.01$ m/sK, $L_v = 1.08$ GJ/m^3, $T_M\Gamma = 1.0(10^{-7})$mK, and V = 1 m/s, we find that the interface is unstable for $\omega < 1.6(10^4)$ m^{-1}; the maximum value of the real part of σ occurs at $\omega = 8(10^3)$ m^{-1} with $\sigma = [2.9(10^3) + i\ 2.5(10^4)]$ s^{-1}. Thus, for either sign of $\mu_A - \mu_T$, the interface is unstable for small values of ω and is stabilized by surface tension for large values of ω; however, for $(\mu_T - \mu_A) < 0$ the nature of the instability is oscillatory. The treatment by Temkin and Polyakov[19] did not uncover these oscillatory instabilities because it used steady state heat flow equations.

IV. Growth into Undercooled Melts

Solidification into undercooled melts ($G_L<0$) deserves special attention because for this case, the constitutional supercooling principle always predicts instability. As shown below, the interface can be stable under these conditions for sufficiently large values of G_s. In the thermal steady state approximation, the previous analysis, equations 6 and 7, is still valid as long as $k_sG_s + k_LG_L = 2k_LG_L + VL_v > 0$; however, if this inequality does not hold, equation (6) predicts instability as $\omega \to 0$. This suggests that a more rigorous analysis is required since the thermal steady state approximation assumes that $\omega >> (V/2\kappa_s)$ and $\omega >> (V/2\kappa_L)$.

We let $\sigma \to 0$ and define the quantity $R(\omega) = \{-k_LG_L(\alpha_L-V/\kappa_L) - k_sG_s(\alpha_s+V/\kappa_s)\}/\{2\bar{k}\,\bar{\alpha}\}$. If $R(\omega) < 0$, the thermal field is stabilizing while for $R(\omega) > 0$ the thermal field is destabilizing. Clearly $R(0) = -G_sk_s\kappa_L/(k_L\kappa_s)$ and $R(\infty) = (-k_LG_L-k_sG_s)/2\bar{k}$ and these have opposite signs when $k_LG_L + k_sG_s < 0$. These results indicate that the thermal field is stabilizing for very small ω (provided $G_s > 0$) and is destabilizing for large ω (when $k_LG_L + k_sG_s < 0$).

The special case of $G_s = 0$ requires a more delicate analysis which we undertake only for $k_L = k_s$ and $\kappa_L = \kappa_s$. Then $R(\omega) = (-G_L/2)\{1 - [1+(2\kappa\omega/V)^2]^{-\frac{1}{2}}\}$ is a monotonically increasing function of ω with $R(0) = 0$ and $R(\infty) = (-G_L/2) > 0$. Hence, the thermal field is destabilizing in this case. Since the solute field is always destabilizing and surface tension is important only for large ω, we conclude that such a situation is unstable.

In applying such an analysis to the solidification of supercooled droplets, there is an additional factor that needs to be considered, viz., that in a small droplet only rather large values of ω can occur. If the droplet is of radius R, then the largest meaningful perturbation wavelength $\lambda = 2\pi/\omega \leq 2R$ or $\omega \geq \pi/R$. Thus, for a droplet of 1 μm diameter $\omega \geq 6(10^6)m^{-1}$ so that $\omega > V/2\kappa_L$ even for velocities of the order of 1 m/s. Thus, $R(\omega) \sim (-k_LG_L/2\bar{k})$, and the surface tension term $T_M\Gamma\omega^2 \geq 3.6(10^6)K/m$. For $G_L > -1.2(10^7)K/m$ or $V < 1.0$ m/s, we would expect a stable interface for the solidification of a droplet of pure aluminum. When solute is present, the magnitude of the surface tension term must be sufficiently large to overcome the destabilizing temperature and solute gradient terms. Numerical calculations with $G_s = 0$ and $\omega \geq 6(10^6)m^{-1}$ yield critical concentrations of 0.12, 0.028, and $7.7(10^{-4})$ wt. % for velocities of 0.01, 0.1, and 1.0 m/s, respectively. If we take $\sigma/V = 10^6$ m^{-1} rather than zero, we find critical concentrations of 0.15, 0.038, and 0.034 wt. % for velocities of 0.01, 0.1, and 1.0 m/s, respectively with $\omega = 6(10^6)$ m^{-1} as limited by the particle radius. For $\sigma/V = 10^7$ m^{-1}, ω is

no longer limited by the particle radius and we find critical concentrations of 2.34, 0.37, and 0.33 wt. % with $\omega_m = 1.5(10^7)$, $1.7(10^7)$, and $2.9(10^7)$ m^{-1} for V = 0.01, 0.1, and 1.0 m/s, respectively, Thus, although an undercooled melt with $G_s = 0$ is unstable, strictly speaking, for any composition, some minimum composition is needed for this instability to be observed in small droplets because of capillary stabilization.

V. Discussion

We have demonstrated in some detail how the principle of constitutional supercooling and morphological stability theory can lead to quite different results at rapid solidification rates. In particular, this occurs because of increased capillary stabilization of the short-wavelength perturbations important at high velocities (absolute stability), because of increased departures at the solid-liquid interface from local equilibrium, and because of the important role of the temperature gradient in the solid in the case of undercooled melts. We have also presented some numerical calculations that illustrate the refinements in the growth conditions needed to observe instabilities in the cases of solidification of thin films and fine droplets. These effects suggest the need for more careful experimental observations at rapid solidification rates.

We emphasize that all of the above conclusions are based on the use of macroscopic transport theory. Surely, when solidification rates become so rapid that critical lengths, such as D/V, become the order of atomic dimensions, the use of macroscopic transport theory cannot be justified. For Cu in Al, D $= 5 \times 10^{-9}$ m^2/s and D/V would be less than 10Å for V > 5 m/s. The critical wavelength for instability is greater than D/V for large V; thus, D/V is the length with which we have to be concerned. As we have seen, departures from local equilibrium can be handled in a formal way but there is little known about exact forms and magnitudes of these departures. We caution again that our results are only strictly applicable to constant V; the case of large but time-dependent V is probably prevalent in most experiments that involve rapid solidification rates and remains as a ripe subject for further research.

Acknowledgements

The authors are grateful for partial support from the Defense Advanced Research Projects Agency and (for RFS) to the National Science Foundation under Grant DMR78-22462. Gratitude is also expressed to Drs. W. J. Boettinger, J. W. Cahn, R. Mehrabian, R. G. Rehm and R. J. Schaefer for helpful discussions.

References

1. W. A. Tiller, J. W. Rutter, K. A. Jackson, and B. Chalmers, Acta Met., Vol. 1, p. 428, 1953.

2. W. W. Mullins and R. F. Sekerka, J. Appl. Phys., Vol. 34, p. 323, 1963.

3. W. W. Mullins and R. F. Sekerka, J. Appl. Phys., Vol. 35, p. 444, 1964.

4. V. V. Voronkov, Sov. Phys. Solid State, Vol. 6, p. 2378, 1965.

5. R. F. Sekerka, Crystal Growth: An Introduction, p. 403, edited by P. Hartman, North-Holland, Amsterdam, 1973.

6. A. A. Chernov, Sov. Phys. Crystallogr., Vol. 16, p. 734, 1972.

7. R. T. Delves, Crystal Growth, Vol. 1, p. 40, edited by B. R. Pamplin, Pergamon, Oxford, 1974.

8. D. J. Wollkind, Preparation and Properties of Solid State Materials, Vol. 4, p. 111, edited by W. R. Wilcox, Marcel Dekker, New York, 1979.

9. J. S. Langer, Rev. Mod. Phys., Vol. 52, p. 1, 1980.

10. H. S. Chen and K. A. Jackson, J. Crystal Growth, Vol. 8, p. 184, 1971.

11. J. S. Wey, A. K. Gautesen and J. Estrin, J. Crystal Growth, Vol. 19, p. 169, 1973.

12. R. F. Sekerka, Crystal Growth, p. 691, edited by H. S. Peiser, Pergamon, Oxford, 1967.

13. D. J. Wollkind and R. N. Maurer, J. Crystal Growth, Vol. 42, p. 24, 1977.

14. R. F. Sekerka, J. Appl. Phys., Vol. 36, p. 264, 1965.

15. S. R. Coriell, D.T.J. Hurle and R. F. Sekerka, J. Crystal Growth, Vol. 32, p. 1, 1976.

16. L. R. Morris and W. C. Winegard, J. Crystal Growth, Vol. 5, p. 361, 1969.

17. S. R. Coriell and R. F. Sekerka, J. Crystal Growth, Vol. 34, p. 157, 1976.

18. J. W. Cahn, Japan-U.S. Joint Seminar on Solidification of Metals and Alloys, Jap. Soc. for the Promotion of Science, Tokyo, Japan, p. 1, 1977.

19. D. E. Temkin and V. B. Polyakov, Sov. Phys. Crystallogr., Vol. 21, p. 374, 1976.

EUTECTIC SOLIDIFICATION AND THE FORMATION OF METALLIC GLASSES

W. J. Boettinger, F. S. Biancaniello, G. M. Kalonji and J. W. Cahn

Metallurgy Division
Center for Materials Science
National Bureau of Standards
Washington, DC 20234

ABSTRACT

The relationship between eutectic solidification and the ease of formation of metallic glasses is investigated. For many systems, crystallization, including partitionless crystallization, of alloys into a single phase solid is impossible over a wide range of composition near stable or metastable eutectics. This fact forces alloys to crystallize into two-phase solids. Because of the need for diffusional sorting of the components and creation of solid-solid surfaces, the kinetics of eutectic crystallization are relatively slow and may be closely related to the ease of glass formation of these alloys.

Experiments are reported on the directional solidification of Pd-6 at % Cu-17 at % Si alloys which show the evolution of microstructure as a function of interface velocity. A structure of dendrites and interdendritic eutectic at low velocity ($\lesssim$ 0.25 mm/s) becomes a fine eutectic-like structure at intermediate velocities ($\sim$ 1 mm/s) and finally the alloy forms glass when crystallization is attempted at velocities greater than 2.5 mm/s.

Introduction

Eutectic systems are multicomponent systems in which liquid remains the equilibrium phase to low temperatures because no solid with the same composition is stable. Because of the stability of the liquid at low temperatures these systems have been prime candidates for glass formers by rapid solidification. The theory and practice of how rapidly one needs to solidify has primarily focussed on the nucleation and growth of a single solid phase as the difficult step in crystallization (1-3). We have focussed instead on the coupled growth of two (or more) solid phases.

There are two aspects being explored: 1) the thermodynamic question for each system of the absence of a solid phase with the same composition as the liquid which at some temperature below the eutectic becomes stable relative to the liquid, 2) the kinetic question of how fast a liquid can crystallize into mixtures of crystals of differing composition. The diffusional sorting of the components is a relatively well understood slow step which governs the crystallization rate. These ideas have led to a series of predictions for such systems which are being explored experimentally.

The thermodynamic question is best answered by examination of the position of the T_0 curves (4) for all possible solid phases on the phase diagram. A T_0 curve is the intersection of the solid and liquid free energy curves plotted on a phase diagram. It marks the bound on compositions of a solid phase which can form from liquid of any composition at that temperature. Figure 1a shows a hypothetical phase diagram with a stable and a metastable eutectic. If the composition range of an individual phase is very narrow or if the solidus is retrograde (5), the T_0 curves will not extend far from that phase at temperatures of interest. This produces a rather wide range of alloy compositions between the T_0 curves of the different phases which must crystallize as two-phase solids. Even partitionless (massive) crystallization of liquids in this composition range into a single phase is impossible. Wider composition ranges requiring two phase crystallization are possible if a particular phase fails to nucleate (for example, β in Figure 1a).

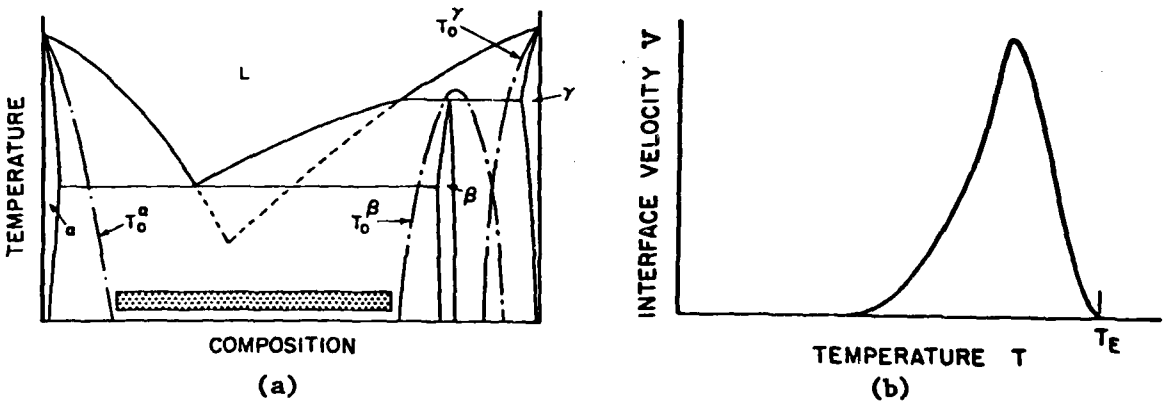

Figure 1. a) Hypothetic phase diagram with a stable and a metastable eutectic. The T_0 curves for the three solid phases relative to the liquid are shown. In the shaded region of composition between T_0 curves, crystallization to a single phase crystalline solid is impossible. b) Relationship of interface temperature to interface velocity for coupled growth of two phases. T_E is the eutectic temperature.

The growth of a two-phase solid from the liquid requires the diffusional sorting of the components in the liquid phase as well as the creation of new surface area between solid phases. These requirements for coupled growth lead to well known relationships (6,7) between interface undercooling ΔT below the eutectic temperature, interface velocity V and eutectic spacing λ; namely,

$$V = \frac{D(T)(\Delta T)^2}{4A_1A_2} \quad , \tag{1}$$

$$\lambda^2 V = \frac{D(T)A_2}{A_1} \quad , \tag{2}$$

and redundantly

$$\lambda = 2A_2/\Delta T. \tag{3}$$

Here D(T) is the interdiffusion coefficient in the liquid which is a strong function of interface temperature at large undercoolings. The parameters A_1 and A_2 are approximated by $m\Delta C/8$ and $2\gamma_{\alpha\beta}/\Delta S$, respectively, where m is an average positive liquidus slope, ΔC is the composition difference between the solid phases, $\gamma_{\alpha\beta}$ is the α-β surface energy and ΔS is an average entropy of fusion of the solid phases. The above equations use the extremum principle although refinements of this aspect are possible (8). Extension of eutectic solidification theory to ternary systems has been performed (9) and leads to similar results.

For a given interface velocity, the interface undercooling required for eutectic solidification based on equation (1) is much greater than for single phase crystallization. In fact for this reason, interface attachment kinetics are neglected in equation (1). For example, for velocities of 10 μm/s one expects undercoolings of the order of 10^{-4}K (10) for single phase crystallization of metals, whereas for eutectics such a velocity would lead to an undercooling of the order of 1K (11). For larger interface velocities the temperature dependence of the diffusion coefficient becomes very important and the undercooling becomes much larger. Figure 1b shows schematically the form of Eqn. 1 for a diffusion coefficient with Arrhenius behavior. A maximum velocity exists beyond which eutectic solidification cannot occur. Such a maximum also occurs for single phase solidification but it occurs at a much higher velocity. Similarly, minimum transformation times from time-temperature transformation curves have been calculated by Boswell & Chadwick (12). Alloys required to crystallize at velocities greater than this maximum due to the rate of heat extraction and which cannot crystallize as a single phase material will undoubtedly form a glass.

The purpose of this research is to determine whether this prediction of a maximum crystallization velocity for a eutectic is related to the ease with which certain alloys form glass. Preliminary experiments are reported in which a glass-forming alloy has been directionally solidified at various interface velocities. Alloy microstructure including the transition to the glassy state is described as a function of interface velocity.

Experiments

Rapid directional solidification is being conducted by quenching thin alloy-filled quartz tubes (0.75 mm I.D. x 1.5 mm O.D. x 10 cm long) from a furnace at 1100 °C into liquid Ga at various controlled speeds. Samples are initially lowered at 0.25 mm/s to obtain about 3 cm of crystalline solid. This step prevents bulk undercooling of the liquid and permits study of the growth aspects of the alloy unencumbered by nucleation difficulties. Samples are then quenched at the desired speed. An important consideration here is whether the interface velocity is equal to the quenching rate. Care was taken in the present experiments to maximize the extraction of heat from the samples during quenching by the use of thin samples with thin container walls and a high boiling point quenchant. If the heat flow is directional and parallel to the tube axis in the alloy, the interface velocity must be less than or equal to the quenching rate. In fact an initial transient where the interface accelerates to the quenching speed was expected and observed microstructurally to be about 2 cm long.

The alloy chosen for this research is Pd-6 at % Cu-17 at % Si because of its well known ease of glass formation. Unfortunately, the Pd-Si as well as the Pd-Cu-Si phase diagrams are not well known (13-15). Figure 2a and 2b show micrographs of this alloy solidified at 0.25 and 1.0 mm/s, respectively. Both samples show strong alignment of microstructure parallel to the tube axis and indicate directional heat flow for this geometry and these quenching speeds. At 0.25 mm/s (Fig. 2a) the microstructure consists of both faceted and unfaceted dendrites and an interdendritic two phase eutectic. Suprisingly both types of dendrites appear to be the same phase and have a composition, determined by electron microprobe, of 78 at % Pd, 20.6 at % Si and 1.4 at % Cu and an electron diffraction pattern which has been indexed based on an orthorhombic cell with a = 7.46Å, b = 9.27Å and c = 9.60Å. The phase occurring along with this phase in the eutectic has a composition 73 at % Pd, 12.1 a/o Si and 14.9 a/o Cu and appears to have cubic symmetry.

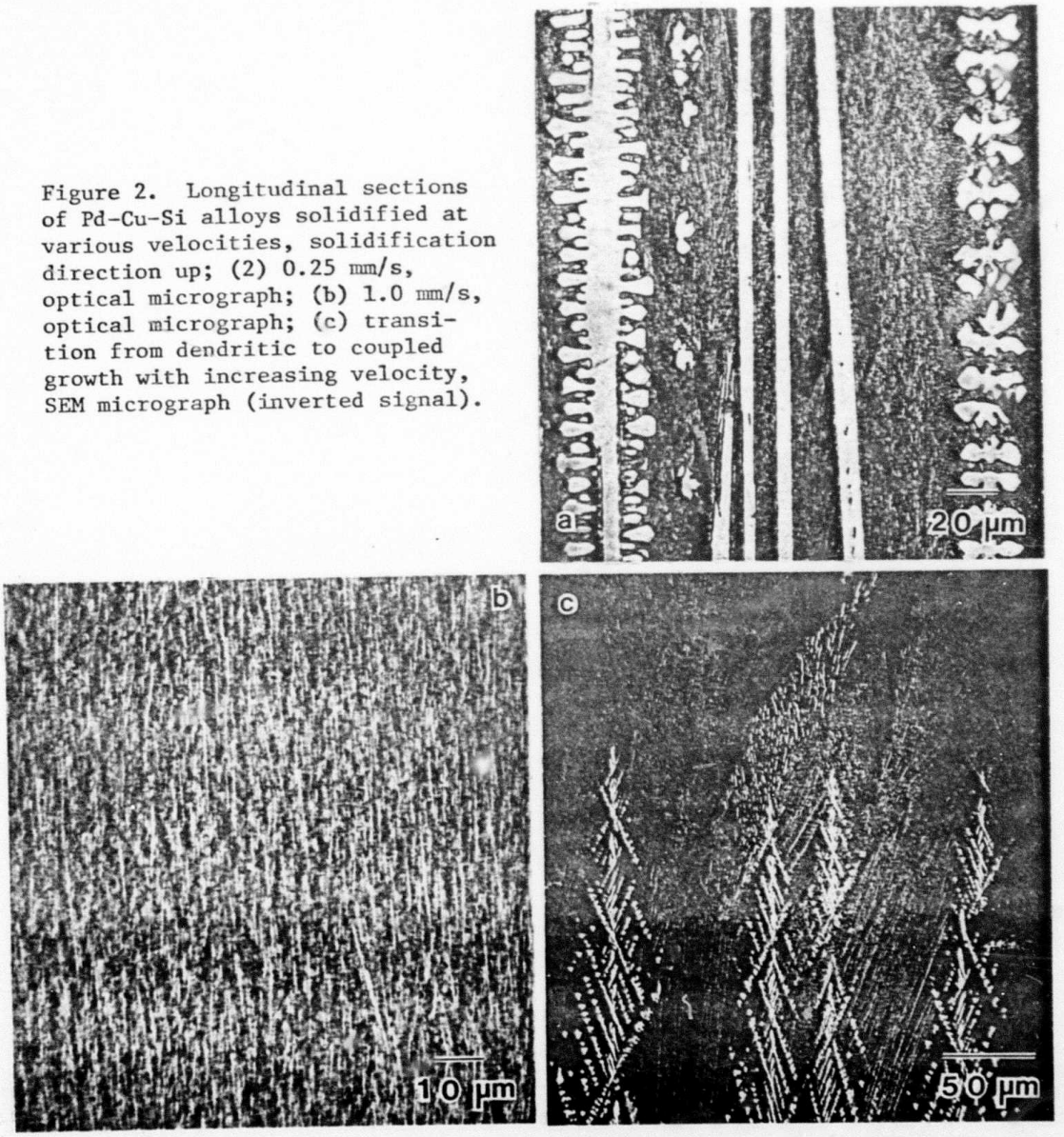

Figure 2. Longitudinal sections of Pd-Cu-Si alloys solidified at various velocities, solidification direction up; (2) 0.25 mm/s, optical micrograph; (b) 1.0 mm/s, optical micrograph; (c) transition from dendritic to coupled growth with increasing velocity, SEM micrograph (inverted signal).

At 1.0 mm/s the dendritic phase is absent and the microstructure consists of a fine eutectic structure as shown in Figure 2b. A complete characterization of this structure is currently underway. The transition from dendritic to fine eutectic structure with increasing velocity is quite significant. This transition is shown dramatically in Figure 2c which occurred in the initial transient region of the sample quenched at 1 mm/s. Similar transitions from dendritic to eutectic-like structures with increasing velocity have been observed in off-eutectic Pb-Sn alloys by Cline and Livingston (16). It appears that alloys over a range of compositions near eutectics can undergo coupled growth of two or more phases at high velocity. Hence the kinetic treatment presented in the Introduction applies.

Alloys quenched at 2.5 mm/s exhibit a very different microstructure — they are amorphous. In the initial transient there is the transition from dendritic to coupled growth already described, a refinement of the eutectic spacing and then a sharp interface as shown in Figure 3a. The light region above the sharp interface is featureless and has been determined to be glassy from its x-ray and electron diffraction patterns. The glassy region extends the remaining 5 cm length of the sample and occupies the region where steady state interface speed is ordinarily observed. It is believed that the general vicinity of the sample shown in Figure 3a represents the place where the interface velocity reached the maximum shown in Figure 1b. The transition from the dark to gray-etching area below the glass interface represents a dramatic reduction in the eutectic spacing. However, the structure appears to remain eutectic-like right up to the glass interface as seen in Figure 3b. This region of fine eutectic spacing may possibly be the material that crystallized on the part of the kinetic curve (Fig. 1a) with positive slope. A small star-shaped dendrite visible in Figure 3a formed in this region, possibly due to large liquid undercooling, but was overtaken by the eutectic interface.

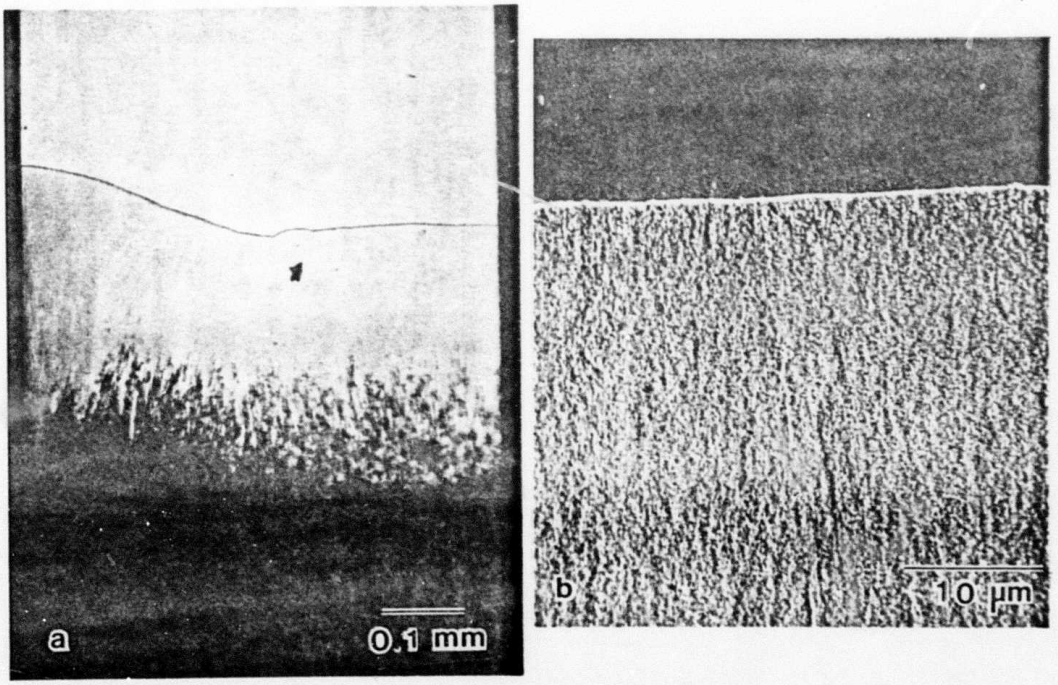

Figure 3. Transition from fine eutectic growth to glassy alloy observed when crystallization at 2.5 mm/s is attempted, optical micrograph, entire sample width. (b) SEM view of interface between fine eutectic structure and glass.

A conclusion of this paper is that the maximum velocity of eutectic solidification of this alloy is between 1.0 and 2.5 mm/s. Attempts to crystallize at velocities greater than this lead to glass formation. We have also seen similar sharp interfaces between fine eutectic structures and glass in electron-beam surface melted samples.

Future work will include attempts to measure interface temperature, temperature gradient, and eutectic spacing along with an identification of the phases present during eutectic solidification at velocities just below the transition to the glass. This information will permit a semi-quantitative evaluation of Eqn. 1.

Acknowledgements

Support of this work by the Defence Advanced Research Projects Agency along with the constructive suggestions of M. Kuriyama, S. R. Coriell, R. Mehrabian and R. J. Schaefer are greatly appreciated. The metallography was performed by C. H. Brady and D. B. Ballard.

References

1. D. Turnbull, Contemp. Phys., Vol. 10, p. 473, 1969.

2. D. Turnbull, J. de Physique, Colloque No. 4, p. C-4.1, 1974.

3. D. R. Uhlmann, J. Non-Cryst. Solids, Vol. 25, p. 43, 1977.

4. J. C. Baker, and J. W. Cahn, "Thermodynamics of Solidification", Solidification, ASM, p. 23, 1971.

5. J. W. Cahn, S. R. Coriell, W. J. Boettinger, "Rapid Solidification", Laser & Electron Beam Processing of Materials, edited by C. W. White and P. S. Peercy, Matls. Res. Soc., Nov. 1979 (in press).

6. K. A. Jackson and J. D. Hunt, Trans. AIME, Vol. 236, p. 1129, 1966.

7. W. A. Tiller, "Liquid Metals and Solidification", ASM, p. 276, 1958.

8. J. S. Langer, Rev. Mod. Phys., Vol. 52, p. 1, 1980.

9. W. J. Boettinger, PhD Thesis, The Johns Hopkins University, 1972.

10. See for example, M. C. Flemings, Solidification Processing, McGraw-Hill, New York, p. 307, 1974.

11. R. M. Jordan and J. D. Hunt, Met. Trans., Vol. 3, p. 1385, 1972.

12. P. G. Boswell and G. A. Chadwick, J. Matl. Science, Vol. 12, p. 1894, 1977.

13. R. P. Elliott, Consitition of Binary Alloys, First Supplement, McGraw-Hill, New York, p. 732, 1965.

14. E. Roschel and C. J. Raub, Z. Metalkande, Vol. 62, p. 840, 1971.

15. T. B. Massalski, private communication.

16. H. E. Cline and J. D. Livingston, Trans. Met. Soc. AIME, 245 p. 1987, 1969.

THERMODYNAMICS OF METASTABLE EQUILIBRIA

J. W. Cahn

Center for Materials Science
National Bureau of Standards
Washington, DC 20234

ABSTRACT

The thermodynamics of metastable phase equilibrium is closely related to that of stable phase equilibrium. Metastable phase equilibrium can often be represented by extensions of the curves on phase diagrams that represent stable phase equilibria. Thermodynamic principles rank phase equilibria but not phases in a hierarchy of increasing stability. Thermodynamics imposes precursor rules in multicomponent systems in which a prior reaction is required before a phase can appear. A given hierarchy persists over a domain on the phase diagram bounded by surfaces on which the ranking of two equilibria changes. Multicomponent phases per se do not form a hierarchy because a given phase can disappear and reappear in a sequence of spontaneous processes. Processing for producing metastable phases must place the system within a domain in which the desired phases can form spontaneously from the available phases.

Introduction

Thermodynamics is the science of the impossible. It enables us to tell with certainty what cannot happen, but is noncommittal about the things that are possible. Thermodynamics is at its best when nothing more can happen, a condition called equilibrium. The concept of equilibrium has been fruitfully extended to reversible processes which are on the verge of being impossible.

When a system is not at equilibrium, thermodynamics retains its certainty about the impossible. However, the domain of the thermodynamically possible may be so large that thermodynamics has lost much of its usefulness as an aid to prediction. In a complicated nonequilibrium system such as we often encounter in rapid solidification, thermodynamics would be almost totally useless if applied to the entire system, for then an irreversible process in one part, combined with an impossible process in another, could lead to an overall reduction in the appropriate thermodynamic potential and a verdict of "possible". Hence, it is a common assumption that we apply thermodynamics locally, unless we know specifically that there are long-range interactions. Similarly, we often assume that different processes are independent, and apply thermodynamic criteria to each individually.

Another important assumption is that of constrained equilibrium, in which certain processes are assumed not to occur or to occur so slowly that thermodynamics is fully applicable to all the other processses remaining. These three assumptions permit us to apply thermodynamics locally and to individual processes, but the validity of such assumptions must be checked experimentally.

An example of constrained equilibrium is metastable phase equilibrium. Here, the constraint is that one or more of the stable phases is absent. The phases that are actually present reach equilibrium subject to this constraint. This definition of metastable phase equilibrium focusses on the absence of one or more of the equilibrium phases, and does not ascribe any unusual characteristic to the metastable ones present.

A second example of constrained phase equilibrium occurs when the solidification is so rapid that one or more of the components cannot redistribute among the phases in the time scale of the experiment. In a completely partitionless solidification to a single solid phase, the temperature where the liquid and solid have equal free energies traces out a surface (T_o) on the multicomponent phase diagram between the liquidus and solidus for that phase and its extrapolation. Below this surface, provided diffusion is limited, it becomes thermodynamically possible to solidify a liquid completely even though the system may be above its solidus.

In this paper we will focus on metastable equilibria and partitionless (sometines called massive) transformations, their representation on phase diagrams and the hierarchical laws governing the thermodynamically possible sequences of phases and metastable phase equilibria. Certain basic concepts and relationships described in earlier reviews (1,2) and standard textbooks will be assumed. We begin with the single component case and highlight the major complications introduced for multicomponent systems.

Metastable Phase Equilibria in Single Component Systems

A single phase can reach a metastable phase equilibrium when nothing more is possible except the formation of new phases. Nucleation theory tells us that there are natural barriers to the formation of new phases from metastable ones. The range of conditions under which a phase can be metastable is bounded by kinetic factors, imposed by nucleation and growth, and thermodynamic limits commonly called spinodals.

What is important is that it is reasonable to assume that there are no discontinuities in thermodynamic properties as a phase moves from stable to metastable. The same thermodynamic measurements that are made on stable phases can be, and have been, made on metastable phases. Heat capacity, volume, vapor pressure, and other such properties are rigorously defined and have been measured. From such measurements, energy, entropy, and free energy can be rigorously determined. Metastable phases obey the usual solution laws. If they are dilute, Henry's and Raoult's laws apply. They can even be ideal: to wit, a supersaturated vapor at a density far below the critical-point density.

In a single component system phases are in equilibrium when the chemical potentials μ of the component, which in this case are the same as the molar Gibbs free energies, in the several phases are equal. A graph of the free energies of several phases as a function of temperature at constant pressure is shown in Figure 1. At each temperature the stable phases are the ones with the lowest value of F. Consistent with the phase rule only one phase is stable except where the two lowest curves cross. All other phases are metastable. With changing pressure the free energy curves will shift at a rate proportional to the volumes of each phase and different phases may become stable.

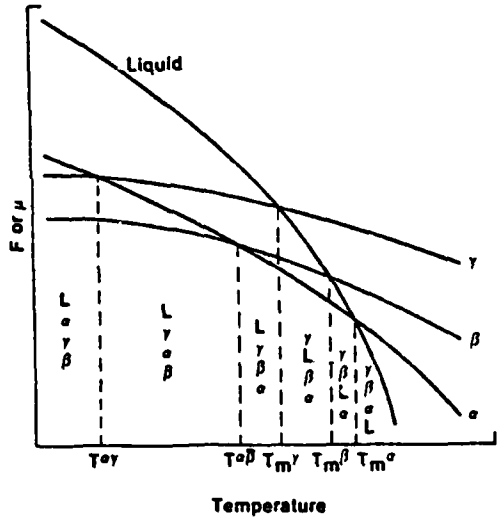

Figure 1. Chemical potential (free energies) of various one-component stable and metastable phases as a function of temperature at constant pressure. The stable phase at each temperature is the one with the lowest μ. Stable and metastable two-phase equilibria occur where two curves cross. Between crossings the hierarchy of phases ranked according to their values of μ is listed.

A graph of the domains where each phase is stable is called a phase diagram and is shown in Figure 2. It consists of areas in which a phase is stable bounded by curves in which two phases are the equilibrium. Three curves come together at triple points of three-phase equilibrium. Vapor-liquid critical points where a two-phase curve terminates are of little concern in rapid solidification. The axes can be any two independent combinations of T, P, or μ.

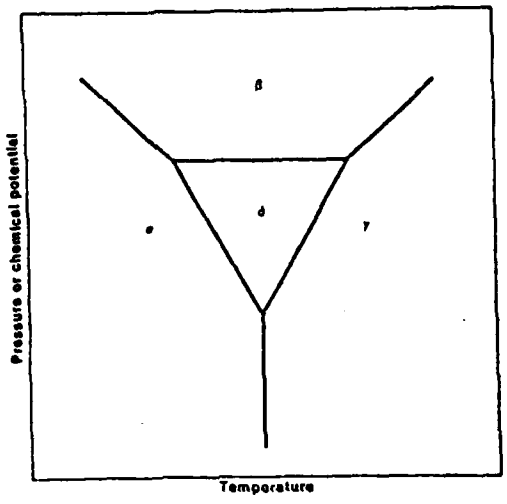

Figure 2. A one-component phase diagram with T. P. or μ as axes, showing stable two and three-phase equilibria as curves and (triple) points.

Equilibria between metastable phases can also be mapped on phase diagrams. Each of the curves in the metastable phase diagram represents a crossing of two free energies. As in the case of the stable diagram each curve is identified with the equilibrium of the two phases, one of which is stable on one side of the curve, the other is stable on the other. In Figure 3 this sidedness of each curve has been identified by labelling the stabler phase on each side. The properties of these two-phase equilibria are unaffected by whether or not there exists a more stable phase. If in some part of the diagram the two-phase equilibrium is stable, the curve representing it can be extrapolated beyond the triple point where it becomes metastable. The stable triple points also have become the crossings of three two-phase curves. The six rays emanating from a stable triple point are alternately stable and metastable.

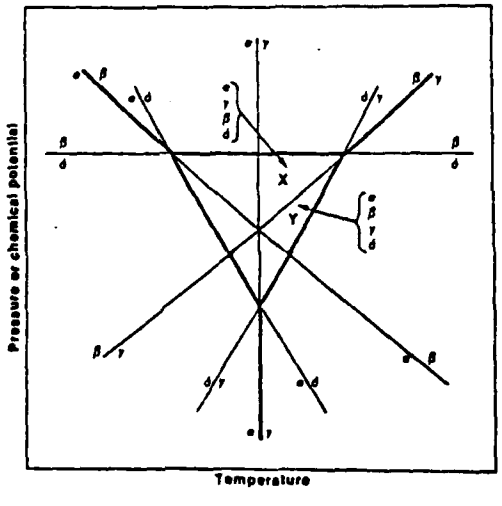

Figure 3. A metastable phase diagram with the same phases as shown in Figure 2. Triple points have become triple crossings with metastable equilibria indicated by light lines. Within each region a given phase hierarchy persists.

Such a metastable phase diagram also features points where three metastable phases are in equilibrium and where three two-phase curves cross.

The metastable diagram is seen to consist of many regions bounded by no more than three curves. Within each region there is a definite hierarchy of phases according to their free energies which is unchanged over the entire region. At a bounding curve a pair of phases change place in the hierarchy and a different hierarchy exists in each adjacent region. In region X the phase hierarchy is $\alpha \rightarrow \gamma \rightarrow \beta \rightarrow \delta$, while in region Y the order of β and γ have been reversed by the traversing of the metastable $\beta - \gamma$ equilibrium curve.

Each triple point represents a place there three phases have equal μ. Three two-phase equilibria curves representing the three pairings of the three phases must cross there. The crossings of two curves representing two pairs of two phases with none in common are not triple points.

The thermodynamic hierarchy for a one-component system ranks phases by their molar free energies. In a thermodynamic processing path of heating, cooling, and pressure changes, a phase can be retained and moved into a region where it is metastable and above one or more phases in the hierarchy. During spontaneous phase changes it can only move down the hierarchy. A liquid undercooled just below its equilibrium melting curve becomes metastable only with respect to the stable crystal. It does not become metastable with respect to a metastable crystal until it has been brought below the melting curve of the metastable phase. This metastable melting curve can often be observed as a reversible phenomenon, and can often be estimated from the stable phase diagram if the metastable phase becomes stable elsewhere in phase diagrams.

Figure 3 included only phases which were stable in some portion of Figure 2. All curves in Figure 3 are extrapolations of curves from the stable phase diagram. Metastable equilibria as well as the metastable hierarchies of all the phases that are stable in some part of a stable phase diagram are thus easy to estimate. For example, bismuth can be made to crystallize at ambient pressure into a high pressure phase which appears to have a metastable melting point of 175 °C consistent with the metastable extensions in the phase diagram (3). It is not surprising that most observed metastable phases appear as stable phases somewhere in phase diagrams either at different pressure, temperature or with small additions of other components. In order for a phase to be formed by rapid solidification it has to be within a few hundreths eV of the stable phase and it is unlikely that a phase will come that close to the lowest free energy without breaking through at some adjacent pressure, temperature or alloy addition. It is not impossible though. Figure 4 gives a hypothetical case where a metastable phase δ comes close to being stable without ever becoming so, and having a free energy curve which is not parallel to that of any other phase. It is quite straightforward to construct the hypothetical free energy surfaces corresponding to the metastable equilibria of Figure 4.

While there is no singularity in thermodynamic properties of the liquid at any of the stable or metastable melting points, there is a rapid change in heat capacity near the glass transition (4). The heat capacity of the amorphous phase at the glass transition is cooling rate and heating rate dependent but seems at the slowest rates to approach a well behaved reversible limit (5,6). For the faster rates there is a lack of reversibility, but heating and cooling curves can establish an upper and lower bound to the free energy of a glass when its properties depend on its thermal history. The slow cooling limit of the glass transition seems well defined, and indicates that the free-energy curves of glass and liquid merge smoothly, exhibiting only a rapid change in curvature. On phase diagrams, the curves representing the metastable equilibria between the amorphous phase and some other phase are continuous through the glass transition, but exhibit a rapid change in slope. If the metastable crystalline phase does not catalyze the nucleation of a stabler crystalline

phase, the reversible growth or dissolution of this phase in contact with a glass should be observable.

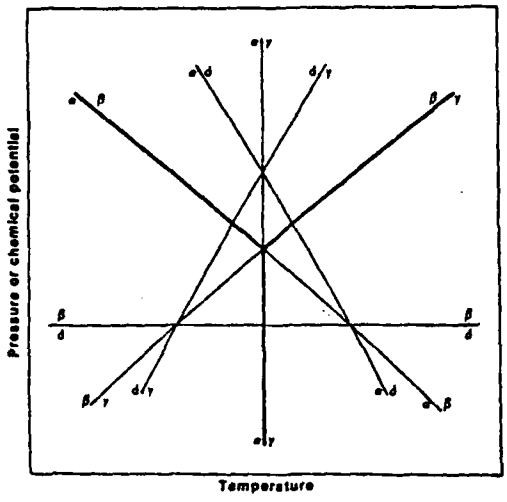

Figure 4. A metastable phase diagram similar to Figure 3 except that the δ-phase is nowhere stable.

Solidification processing permits a climbing in free energy away from the equilibrium. The solidification cycle is not unlike a heat engine. Energy is added at the melting point and the maximum rise in free energy ΔF depends on how far the system can be cooled while retaining the latent heat ΔH. In fact because $\Delta F=\Delta H(\Delta T/T_M)$ the analogy with the Carnot efficiency $(\Delta T/T_M)$ can be made. Like the heat engine, the usable stored free energy is reduced by irreversible processes such as diffusion, heat flow, and interface kinetics. Rapid solidification is a means for forstalling solidification and achieving a high free energy, but its irreversible aspects dissipate much of the available free energy. Slow cooling with controlled nucleation is a very good way of producing glass or highly metastable crystalline phases. In multicomponent solidification slow cooling can through segregation, produce a system with much free energy stored in the wide composition range and in the eutectic phases that would not be part of the equilibrium solid, while rapid segregationless cooling could in one stage produce an equilibrium homogeneous solid. The controlled ability to get either closer to equilibrium or further from equilibrium by rapid solidification through the manipulation of the kinetic and thermodynamic variables must surely be one of the most important attributes of this new processing field.

Multicomponent Phase Equilibria, Partitionless Phase Changes and Metastable Hierarchies

The complications introduced by several components are not obvious at first glance. Metastability of each phase is again common and limited only by spinodals and nucleation and growth kinetics. Thermodynamic properties of metastable phases are well behaved and often smooth extensions of behavior in stable ranges. Equilibria are still dictated by equality of chemical potentials of each component but this no longer implies equal free energies. A phase diagram having as axes T, P, $\mu_2....\mu_N$ or more symmetrically T, μ_1, $\mu_2....\mu_N$ would be a (N+1)-dimensional analogue of the single component diagram where N are the number of components. Single phases would occupy (N+1)-dimensional hyper-volumes, bounded by N-dimensional hypersurfaces representing two-phase equilibria, which intersect at (N-1)-dimensional hypersurfaces representing

three-phase equilibria, etc. until there are points representing (N+2)-phase equilibria. Such a phase diagram is useful for an open system in which material reservoirs keep the chemical potentials fixed by letting compositions change. In a few situations we do impose open system conditions for some of the components by e.g., fixing the partial pressures of a gas containing these components, but more generally, we fix the composition of our system, which leads to profound complications in the thermodynamics. The open-system metastable diagram would be constructed by extension of all two-phase hypersurfaces and would divide the space into simplexes in each of which a hierachy of phase equilibria would exist.

In open systems the entire phase diagram is occupied by single phase hypervolumes with multiphase equilibria occupying hypersurfaces of lower dimension and thus of zero measure. Unless we take pains to fix chemical potentials and temperature to lie precisely on one of these multiphase surfaces, the system will almost always be single phase. If it is multiphase an infinitesimal shift in conditions off the surface will return it to be single phase. The open system metastable phase diagram is a multidimensional version of a one-component phase diagram and the same rules including the hierarchial one apply. Indeed Figures 2-4 could serve as examples of a two-dimensional section of a multicomponent phase diagram.

Major changes occur when we shift to closed systems in which the overall composition rather than the μ's are fixed. This is the usual situation in rapid solidification. Phase diagrams for closed systems have compositions as axes and contain (N+1)-dimensional hypervolumes of one-, two-, and N-phase equilibria with (N+1) and (N+2)-phase equilibria occupying hypersurfaces of zero measure. The same phases remain in equilibrium throughout the volume as temperature, pressure and composition shift.

A common graphic method of depicting the multiphase equilibria is the common tangent hyperplane to the free energy hypersurfaces for the various phases at a given temperature and pressure. It is fully equivalent to the condition of equal chemical potential of all the components, and the range of the line segment between tangent points readily demonstrates how the same two phases can remain in equilbrium over a wide composition range (Fig. 5).

The stable multiphase equilibria are those where the hyperplane tangent to the free energy surface of the equilibrium phase does not cross the free energy surface of any phase. If it does cross, the equilibrium is metastable with respect to the formation of the phase.

It is immediately apparent from Figure 5 that there is a hierarchy of metastable phases denoted by free energy curves (or hypersurfaces) and phase equilibria denoted by tangent line segments (or hyperplanes). The boundaries to a given hierarchy are given first of all by the tangent points on the free energy curves. These tangents map out the stable and metastable phase diagram (Fig. 6).

Three other features mark changes in the hierarchy. The intersections of free energy curves (or hypersurfaces) define the T_0 curve (or hypersurface) which can appear on phase diagrams. It defines a restricted equilibrium for partitionless transformation. The T_0 curves do not denote a stable or metastable equilibrium. They do pass through congruent points on the phase diagram and lie within the corresponding two-phase field. They also intersect at T_0 triple points (or hypercurves) where three phases have the same free energy.

T_1 curves in Figure 6 mark the intersections of tangent planes and therefore form ruled hypersurfaces on phase diagrams. T_2 curves mark the intersection of a surface of one phase with a plane tangent to two others.

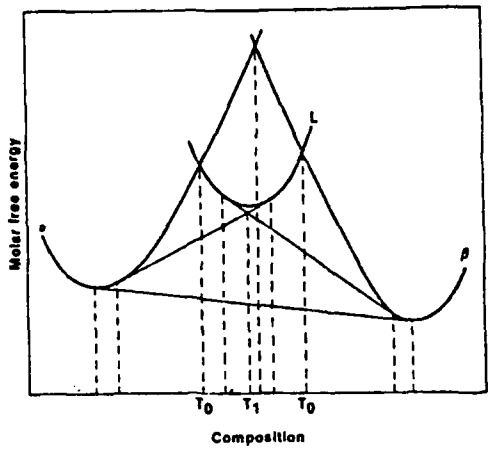

Figure 5. Two-component free energy curves for various phases at constant temperature. The left and right portions of the curves for α and β respectively, and the tangent between them represent the stable equilibrium. Several metastable equilibria are depicted by other tangents. The crossing of free energy curves represent points on the T_0 curves, while the crossing of tangents represent T_1 curves. Within each region of composition separated by the vertical lines a given phase-equilibrium hierarchy holds.

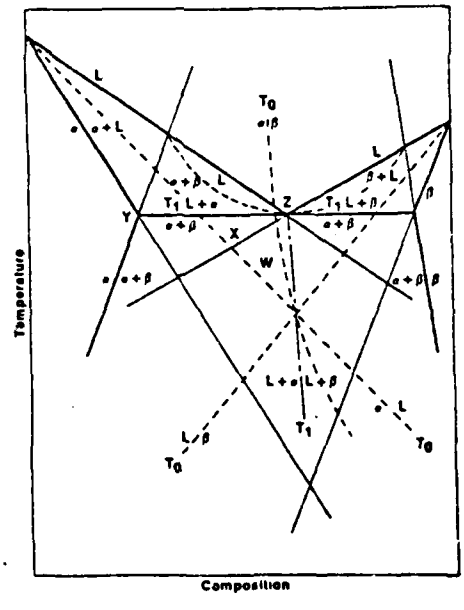

Figure 6. A binary-eutectic diagram at constant pressure with metastable extension of all curves and the T_0 and T_1 curves. Because metastable liquid at point X will dissolve small amounts of the stable phase β, no stability hierarchy based on phases per se can exist.

The features of multicomponent phase diagrams can be readily imagined to originate from free energy surfaces of various phases that evolve and shift relative to each other with changing temperature and pressure. It is seen that the metastable continuation of a stable equilibrium involves only the free energy curves of the participating phases and should be unaffected by the new phase whose free energy surface happened to move through the tangent plane. Thus all stable equilibria can again be extended to depict the metastable equilibria between the same phases. The qualitative evolution of the metastable portion of Figure 6 can be understood by the more rapid rise in Figure 5 of the liquid free energy relative to that of the two solids with decreasing temperature. These free energy curves could be obtained quantitatively by a number of methods and then extrapolated to allow determination of the metastable diagram. For some of the curves it seems far simpler and probably more accurate to extrapolate the portions of a measured stable (or metastable) phase diagram.

As for the single component, wherever a liquid undergoes a glass transition the curves will be continuous with only a rapid change of slope.

It should be immediately pointed out that no simple hierarchy of phases exists. A system at a point in region X in Figure 6 is in equilibrium when α and β are present as the stable phases, and the liquid is metastable. Yet when stable β is brought into contact with liquid in X under conditions where α does not nucleate, stable β will dissolve in metastable liquid. Such a reaction in which a stable phase dissolves in a metastable one is impossible in single component systems, but quite common in multicomponent ones. Only when α finally nucleates can β reappear. This disappearance and reappearance of a phase in spontaneous processes indicates that there can be no hierarchical listing of phases.

This can also be indicated by listing the metastable hierarchies in region X. Because X lies outside the $\beta + L$ field, no equilibrium between β and L is possible. The remaining five equilibria are ranked as follows: single-phase β is highest in free energy, followed by single-phase α, single-phase liquid, two-phase $\alpha + L$, and equilibrium is reached with two-phase $\alpha + \beta$. In region W the sequence $\beta + L$ is inserted between L and $\alpha + L$. In such metastable sequences phases can appear, disappear, reappear with a different composition and disappear again. Once a particular phase equilibrium has disappeared it can not reappear unless the system is reprocessed.

The inability of β to form from liquid in X unless α has also appeared is an example of a thermodynamically required precursor reaction (7). Such requirements do not occur in single component systems, because any of the more stable phases can appear at any time. Consider a multicomponent system in metastable equilibrium of one or more (m) phases. The composition must lie within that m-phase field on the metastable phase diagram. The addition of a new phase can occur only if the composition lies also beyond where the metastable (m+1)-phase field first intercepts the m-phase field. In Figure 6, β can form from liquid in W but not in X, while α can form in either. This places a strong and easily formulated constraint on the phase-sequences that can occur in a given hierarchy which can be locally applied even if the system has only reached local equilibrium.

During such isothermal sequences the free energy is monotonically decreasing, but chemical potentials can increase as well as decrease. In the graphical construction of Figure 5, the chemical potentials of the two components are the intercept with the component axes of a tangent to the single phase curve at the system composition or of the common tangent in a multiphase equilibrium. These ups and downs of chemical potentials of a component go hand in hand with the appearance or disappearance of a phase enriched in that component.

In solidification, thermodynamics put bounds on the solid composition that can form from liquid given the composition and temperature of the liquid at the interface (1). The T_0 curves pertaining to liquid with a given solid form an upper bound to the solid composition that can form from liquid of any composition at that temperature. Because the T_0 lies between the liquidus and solidus, systems in which the extrapolated solidus appears to span the entire composition range are good candidates for segregationless solidification to that particular phase. Systems with retrograde solidi (stable or metastable), even where the corresponding liquidi sweep across the composition axis, can be shown to have T_0 curves which are bounded in composition. Compositions beyond this bound, which is approximately the liquidus composition at the retrograde temperature (8), can not undergo segregationless solidification to that crystalline phase at any temperature. Because crystallization involving segregation is much slower, retrograde systems might be good candidates for glass formers.

Two T_1 curves in Figure 6 intersect at the eutectic point Z. The eutectic horizontal is a stable T_1, the other moving downward in temperature is metastable and defines bounds to conditions where it is impossible for one metastable two-phase equilibrium to follow another. A T_2 curve (not shown) also goes through point Z. It indicates the temperature where eutectic solidification in the absence of a proeutectic reaction first becomes thermodynamically possible although unlikely.

Because of the segregation accompanying most solidification and the slowness of diffusion in the solid state, most solidification processes yield solids in which the individual phases are not homogeneous. The hierarchy diagrams rank equilibria, and homogeneity of a phase is, apart from minor gravitational and defect segregation phenomena, a necessary condition for equilibrium whether stable or metastable. These segregation effects can bring the system into a state there it contains phases that it would not contain in any metastable sequence.

This can be illustrated by an example. A liquid cooled to a point in region Y could at no temperature during its cooling path reach any equilibria other than α, L, L + α. Yet during conventional cooling, segregation will lead to the formation of β and the system as a whole will not reach equilibrium until all the β has disappeared. The hierarchy diagrams can only be used for conventional solidification on a local equilibrium basis. They are more useful for the solid state sequences following a segregationless solidification or a homogenized solid formed by rapid solidification.

The usefulness of metastable equilibrium diagrams lies in the fact that like stable diagrams there are rules for their construction which guide measurement and permit our experience to be organized. The ability to extrapolate and interpolate is one aspect which lets us make rapid strides in sketching in the main feature of such a diagram. When metastable equilibria is reached, thermodynamics can make its full range of predictions. For single components a sequence of equilibria are likely. The possibility of segregation makes it difficult for us to bring in strong predictions about multicomponent systems, except in rapid solidification and on a local level in conventional solidification.

With new techniques of producing phases increasingly far from stable equilibrium, the need for metastable phase diagrams becomes pressing. While extrapolation of curves from stable diagrams has been long used for estimation and T_0 curves have been in use for diffusionless transformation, a systematic approach in a few important systems should prove the usefulness of the ideas presented here in charting processes far from stable equilibrium.

Acknowledgements

I am grateful to Lee Tanner for generously sharing his vast experience in metastable crystallization sequences in metallic glasses, to W. J. Boettinger for penetrating criticism, to D. Turnbull for helpful discussions about the glass transition and to R. Mehrabian for advice and encouragement. This work was partially supported by the Defense Advanced Research Projects Agency.

References

1. J. C. Baker and J. W. Cahn, "Thermodynamics of Solidification," Solidification, p. 23-58, ASM, Metals Park, Ohio, 1971.

2. T. P. Seward, III, "Metastable Phase Diagrams and Their Applications to Glass-Forming Ceramic Systems," Phase Diagrams, Materials Science and Technology, Vol. 1, p. 295-338, edited by A. M. Alper, Academic Press, New York, 1970.

3. J. H. Perepezko, "Crystallization of Undercooled Liquid Droplets," this volume.

4. W. Kauzmann, Chem. Rev., Vol. 43, p. 219, 1948.

5. C. A. Angell and W. Sichina in "Glass Transition and the Nature of the Glass State," edited by M. Goldstein and R. Simha, N.Y. Acad. of Sci. 1976.

6. R. B. Stephens, J. Appl. Phys., Vol, 49, p. 5855, 1978; J. Non-Cryst. Solids, Vol. 20, p. 75, 1976.

7. J. W. Cahn, J. Am. Ceram. Soc., Vol. 52, p. 118, 1969.

8. J. W. Cahn, S. R. Coriell and W. J. Boettinger, "Rapid Solidification," Laser and Electron Beam Processing of Materials, edited by C. W. White and P. S. Peercy, Materials Research Society, November 1979.

RAPID SOLIDIFICATION

J. W. Cahn, S. R. Coriell and W. J. Boettinger
National Bureau of Standards
Washington, D.C.

Rapid solidification phenomena are described in terms of a hierarchy of increasing deviation from equilibrium. Results of morphological stability theory applied to silicon regrowth indicates that factors outside of conventional constitutional supercooling can explain the observed absence of lateral segregation. A model for interface response functions applicable to solute trapping is presented and a thermodynamic limit to the amount of solute trapping, which seems to be operating in some systems, is proposed.

I. INTRODUCTION

All solidification processes, slow or rapid, involve some nonequilibrium effects. With increasing solidification rates deviations from equilibrium tend to become more extreme. The extent of disequilibrium, however, is nonuniform and different nonequilibrium phenomena become important at widely differing rates. We shall adopt a scheme of classifying solidification effects by their nonequilibrium aspects.

A. Full Diffusional Equilibrium (Global Equilibrium)

At the very slowest solidification rates, diffusional equilibration can occur. In this state of equilibrium, materials are characterized at any time by constant temperature and chemical potential throughout the dimensions L of a sample; i.e., phases are homogeneous, but there will be discontinuities in composition at the interfaces. This equilibrium requires solid state diffusion over distances of the specimen and hence geological times (L^2/D_s where D_s is the solute diffusion coefficient in the solid phase). The existence and compositions of homogeneous phases are given by stable (or metastable) phase diagrams. This kind of global equilibrium will not be approached in solidification processes, except in extremely small systems such as ultrafine dispersions of droplets. Surprisingly because the time scale for nucleation can also be of geological times, metastable

phases can occur in this regime (1). In classical thermodynamics metastable equilibrium is a full equilibrium and indistinguishable from stable equilibrium except that one or more stable phases are prevented from nucleation (2).

B. Local Equilibrium

This next range of phenomena is characterized by the absence of diffusional equilibration in either solid or melt. Each element of the system is assumed to have reached a state where it can be adequately described by the local state variables of temperature, pressure (stress), and composition. The interface is also in local equilibrium. Temperature and chemical potentials of each species can be assumed continuous across the interface, and thus the limiting compositions of each phase at the interface will be given by a knowledge of the interface temperature and the equilibrium phase diagram, with appropriate corrections for the effect of interface curvature. These limiting compositions then form boundary conditions to the transport equations within each phase and a wide range of solidification processes can be modelled with these assumptions (3). Within each phase local equilibrium can be established in times of the order of the diffusional jump frequency. At the interface depending on orientation and defect structure there are a number of relaxation processes with widely differing time scales (e.g., nucleation of a new layer of crystal), that can lead to early breakdown of local equilibrium there (4).

C. Deviations from Local Equilibrium

Effects due to deviations from local equilibrium at the interface already become obvious in some systems at very small undercoolings and very small interface velocities. For example, dislocation-free crystals in contact with slightly superheated or supercooled melts show no measurable growth rates. With increasing interface disequilibrium, growth or melting will begin (4,5). While the facetted form can be an equilibrium form in contact with a fluid of uniform temperature and chemical potential, a growing facetted crystal rarely is at local equilibrium, since melt isotherms or saturation contours are not likely to follow a facetted shape (4). At equilibrium, segregation of solutes between solution and crystal is independent of interface orientation. Thus the observation of compositional discontinuities in Czochralski grown crystal between regions that grew behind facets (core) and regions that grew behind smoothly curved (off-core) liquid melt interfaces indicates that nonequilibrium interface effects are frequently observed at conventional crystallization

rates (6). The prediction of the extent of nonequilibrium interface phenomena has thus been an important goal which has received renewed attention with the investigation of rapid solidification.

This goal may be summarized by response functions (7) which for example give local growth velocities and solid compositions at the interface as a function of conditions at the interface. These response functions replace local equilibrium conditions at the interface and become the boundary conditions to the transport equations in each phase.

While it is clear that many rapid solidification effects can only be understood if the concept of local equilibrium is discarded, some predictions based on local equilibrium have not been fully explored. In the present paper we describe a) results of morphological stability theory relevant to silicon regrowth at high velocities using local equilibrium and b) results of a model for the interface response functions applicable to solute trapping.

II. MICROSEGREGATION AND STABILITY AT THE SOLIDIFICATION INTERFACE

During the freezing of alloys, a planar solid-liquid interface can become unstable. The solute rejected by the growing crystal can lead to a thin layer of undercooled-liquid surrounding the crystal which then makes the shape unstable with respect to dendrites that could protrude into this thin layer. This leads to a cellular or dendritic interfaces and causes solute microsegregation. The classical theory of constitutional supercooling (3,8) predicts increasing instability with increasing velocity (for constant liquid temperature gradient) and would predict cellular or dendritic solidification for most rapid solidification experiments. There are, however, several assumptions that may not be valid for rapid solidification. (1) Local equilibrium at the interface is assumed to describe quantitatively the amount of solute rejected by the growing crystal. (2) Capillarity and latent heat evolution which could stabilize the interface are neglected. (3) The theory indicates a layer of liquid cooler than its local melting point, but does not show how the growing crystal breaks through to this layer.

Beginning with the work of Mullins and Sekerka (9-12), a method of analysing morphological instabilities has evolved which properly solves the transport equations assuming local equilibrium at the interface or making some allowance for deviation from equilibrium. The principal result is that there is far greater stability during rapid solidification than predicted by constitutional supercooling even if local equilibrium is maintained. The transition between planar and

nonplanar growth during the directional solidification of binary alloys can be calculated from linear morphological stability theory assuming local equilibrium. For constant velocity V solidification in the z-direction, the perturbed solid-liquid interface is of the form

$$z = \delta \exp(\sigma t + i\omega_x x + i\omega_y y),$$

where $\delta \exp(\sigma t)$ is the amplitude and ω_x and ω_y are spatial frequencies of the perturbed interface.[x] If the real part of σ is positive for any perturbation (for any values of ω_x and ω_y), the interface amplitude increases exponentially with time t and the planar interface is unstable. If the real part of σ is negative for all possible perturbations, the interface is stable. The value of σ can be determined by solving the heat flow and diffusion equations with appropriate boundary conditions. Assuming local equilibrium at an isotropic solid-liquid interface, Sekerka (13) found

$$\sigma = V\{-k_L G_L(\alpha_L - V/\kappa_L) + k_S G_S(\alpha_S + V/\kappa_S) - 2\bar{k}T_M\Gamma\omega^2\bar{\alpha} + 2\bar{k}mG_c\bar{\alpha}(\alpha - V/D)/(\alpha - pV/D)\}/\{L_V V + 2\bar{k}mG_c\bar{\alpha}/(\alpha - pV/D)\} \quad (1)$$

with

$$\alpha = (V/2D) + [(V/2D)^2 + \omega^2 + \sigma/D]^{1/2},$$

$$\alpha_L = (V/2\kappa_L) + [(V/2\kappa_L)^2 + \omega^2 + \sigma/\kappa_L]^{1/2}$$

$$\alpha_S = -(V/2\kappa_S) + [(V/2\kappa_S)^2 + \omega^2 + \sigma/\kappa_S]^{1/2}$$

$$\bar{\alpha} = (k_S\alpha_S + k_L\alpha_L)/(2\bar{k}),$$

where κ_L and κ_S are thermal diffusivities of liquid and solid, respectively, k_L and k_S are thermal conductivities of liquid and solid, respectively, D is the liquid diffusion constant (diffusion in the solid is neglected), $\omega = (\omega_x^2 + \omega_y^2)^{1/2}$, $\bar{k} = (k_S + k_L)/2$, G_L and G_S are the unperturbed temperature gradients in the liquid and solid, respectively, G_c is the unperturbed solute gradient i.e., $G_c = Vc_\infty(k-1)/Dk$, k is the equilibrium distribution coefficient, c_∞ is the bulk solute concentration, T_M is the melting point of the planar interface in the absence of solute, Γ the ratio of the solid-liquid surface energy, γ, and the latent heat of fusion per unit volume, L_V, m is the slope of the liquidus line on the phase diagram, and $p = 1-k$.

For a given alloy and specified values of the processing conditions we can calculate numerically σ as a function of ω, $\sigma(\omega)$, from the above equation. Alternatively, we set $\sigma = 0$ and calculate the bulk concentration c_∞ as a function of ω,

$c_\infty(\omega)$. The minimum value of $c_\infty(\omega)$ gives the stability-instability demarcation.

The sign of σ is determined by the sign of the numerator in the above equation since the denominator is always positive. The numerator consists of four terms proportional to G_L, G_s, Γ, and G_c, respectively. For the usual case of positive temperature gradients, the first two terms are negative reflecting the stabilizing influence of the temperature field. The surface tension term is always stabilizing. Instability occurs when the destabilizing solute gradient term is sufficiently large to overcome the stabilizing influence of the temperature gradients and surface tension.

It is usually an excellent approximation to neglect the thermal diffusivity terms in the above equations, i.e., let $\kappa_L \to \infty$ and $\kappa_s \to \infty$. In this limit, Sekerka (14) has shown that the stability criterion is

$$2k_L G_L + VL_V > (k_s + k_L) m G_c S(A,k), \qquad (2)$$

where $S(A,k)$ is a function of the dimensionless variables k and $A=(kT_M\Gamma V^2)/(D^2 m G_c)$. The function $S(A,k)$ can be calculated by solving a cubic equation; among its properties are that $0 \leq S(A,k) \leq 1$, $S(0,k) = 1$ and $S(A > 1,k) = 0$. The stability-instability demarcation for silicon containg arsenic and antimony for $G_L = 200$ K/cm is indicated by the curve in Figure 1.

The following values were used for the calculations;

$k_L = 70\ Jm^{-1}s^{-1}K^{-1}$, $k_s = 22.Jm^{-1}s^{-1}k^{-1}$,

$D = 3\times10^{-8}m^2/s$, $k = 0.3$ (As), $k = 0.02$ (Sb),

$L_V = 4.56\ GJ/m^3$, $T_M\Gamma = 1.3\times10^{-7}$ Km,

$\kappa_L = 3\times10^{-5}m^2/s$, $\kappa_s = 9.4\times10^{-6}m^2/s$,

$m = -440$K/at. fract.(As), $m = -370$ K/at. fract. (Sb).

For a given velocity V for solute concentrations below the curve the planar solid-liquid interface is stable. The straight line with negative slope in the figure is the constitutional supercooling criterion, $mG_c = G_L$ or $c_\infty = G_L Dk/[V(k-1)m]$, for interface stability. This follows from the above equation in the limit $S(A,k) \to 1$, $k_s \to k_L$, and $2k_L G_L >> VL_V$. For Si, it appears that even at modest velocities, the preceding inequality, i.e., $G_L >> 3.26\times10^7 V(sK/m^2)$, is not a good approximation, and the latent heat term in the stability criterion can be important. The straight line with positive slope is the Mullins-Sekerka absolute stability criterion (9),

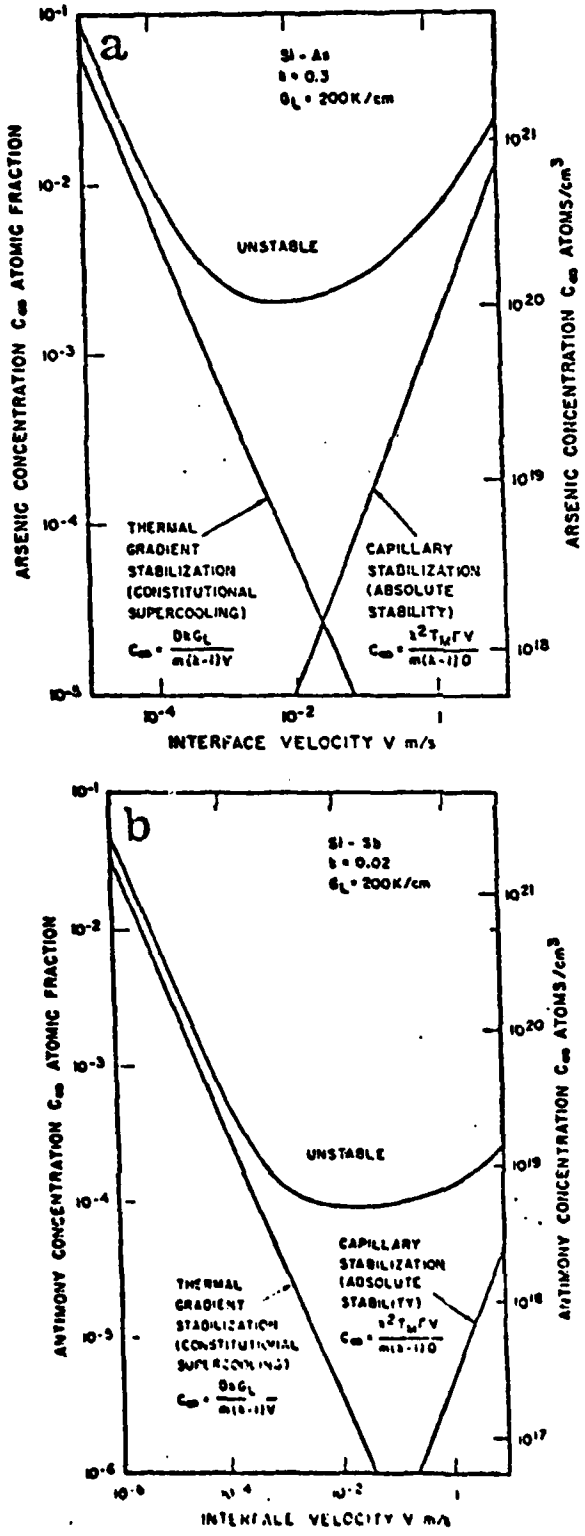

FIGURE 1. The critical concentration of a) As and b) Sb above which interface instability occurs as a function of the interface velocity V of directional solidification of silicon for a temperature gradient in the liquid of 200 K/cm. The curve is based on morphological stability theory while the lines with negative and positive slope correspond to the constitutional supercooling and absolute stability criteria, respectively.

$A=1$ or $mG_c = kT_M r(V/D)^2$ or $c_\infty = k^2 T_M rV/[D(k-1)m]$. For small velocities, the constitutional supercooling criterion is a good approximation to the morphological stability calculations. For very large velocities the absolute stability criterion is a good approximation. Mullins and Sekerka have shown that the exact curve will always lie above the absolute stability line. Thus, for solute concentrations below those given by the absolute stability equation, the interface is stable. Whereas the constitutional supercooling criterion depends linearly on the temperature gradient in the liquid, G_L, the absolute stability criterion is independent of G_L (although we require that $k_s G_s + k_L G_L > 0$). In Figure 2 we show the wavelength, $\lambda = 2\pi/\omega_s$, at the onset of instability as a function of velocity. The wavelength decreases monotonically with increasing velocity. Although we show results for V = 10 m/s, the theory is no longer valid at such high velocities since the diffusion boundary layer length, D/V, is only a few atomic distances.

The theory has been extended to include nonlinear effects (12), some limited interface anisotropy and deviations from local equilibrium (15,16).

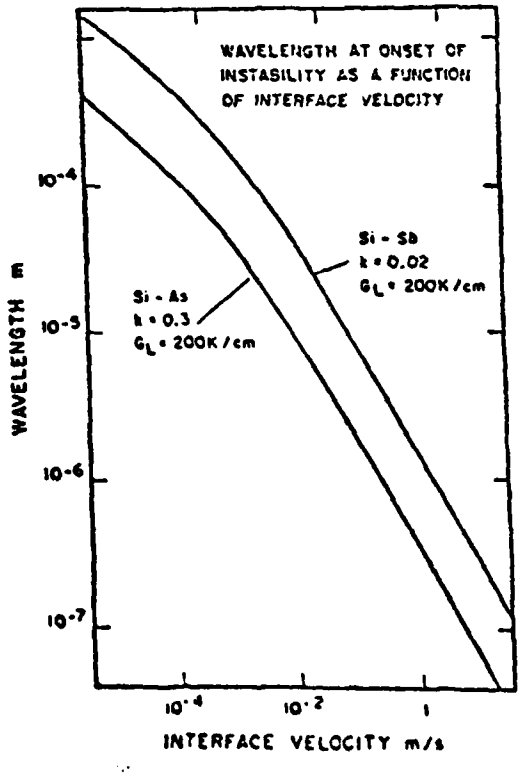

FIGURE 2. The wavelength λ at the onset of instability during directional solidification of silicon containing arsenic or antimony as a function of interface velocity V.

III. NONEQUILIBRIUM AT THE INTERFACE

Crystal growth or dissolution can only occur with some deviation from equilibrium at the interface. The response of the interface to a given deviation from equilibrium has been called the response function (7). Theories attempt to predict for single component systems a relationship between interface undercooling, orientation, crystal perfection, components of interface curvature and the local interface velocity. For a binary system an additional relation is needed to link the solid and liquid compositions to the above variables.

For the single component systems theories have concentrated on mechanisms of crystal growth which broadly fall into two classes: continuous additions to the crystal or lateral spreading of new crystal layers. Crystal perfection only matters for the latter class of mechanisms, in which case imperfect crystals (containing certain types of dislocations or twins) could grow much closer to equilibrium than perfect crystals. A rule based on entropy of fusion and packing on planes parallel to the interface has considerable success in approximately classifying those systems in which lateral growth is likely (17). It has been predicted that at high undercoolings many of these systems change mechanisms and grow by the continuous mechanism (4).

For binary systems an early kinetic theory (18) predicted for the continuous growth mechanism the growth rate and partitioning of solute in terms of four rate constants describing the frequencies with which the two kinds of atoms jump from melt to solid and vice versa. An examination of its predictions showed that this theory predicted that the solid composition could never exceed the equilibrium composition of solid in contact with liquid at the interface temperature (19). To exceed the solid solubility maximum at a eutectic, solidification would have to occur at temperatures where the extrapolated metastable solidus curve exceeded the solid composition. A test of this theory required either knowing the interface temperature during solidification or choosing a system with a maximum in the solidus, a system with retrograde solid solubility. Several such systems have now been examined and the finding of solid solutions in excess of the maximum equilibrium solidus conclusively shows that this kind of theory is inadequate (19-21).

Such a kinetic theory leads to the result that each component must experience a decrease in chemical potential at the interface, if that component is to jump into the solid. The experience with the retrograde systems proves that the minor component can increase its chemical potential upon solidification, a condition termed solute trapping (7,19-21). This condition does not violate thermodynamics and is easily

modelled if one assumes that the solute is passively carried into the solid by the solidification, but can respond to this indignity by diffusing back into the liquid (22). Baker worked out several such models including a fairly interesting one that examined a wide variety of parameters and showed how sensitive the predictions of such models are to minor adjustments.

This model is shown in Figure 3. The interface is a moving snowplow for the solute, whose energy is higher in the solid. Following a suggestion by Chernov (23) that trapping might occur by having the interface be a state of low solute energy to which the solute voluntarily rushes only to be (passively) buried by the addition of the next layer, Baker permitted a variable solute energy at the interface. He also allowed for diffusion in both phases. The resulting continuous steady state diffusion equation with drift term when E is a function of z is readily integrated (24,25) to give the composition profiles as a functional of velocity, E(z) and D(z). Taking the ratio of the limiting compositions of liquid

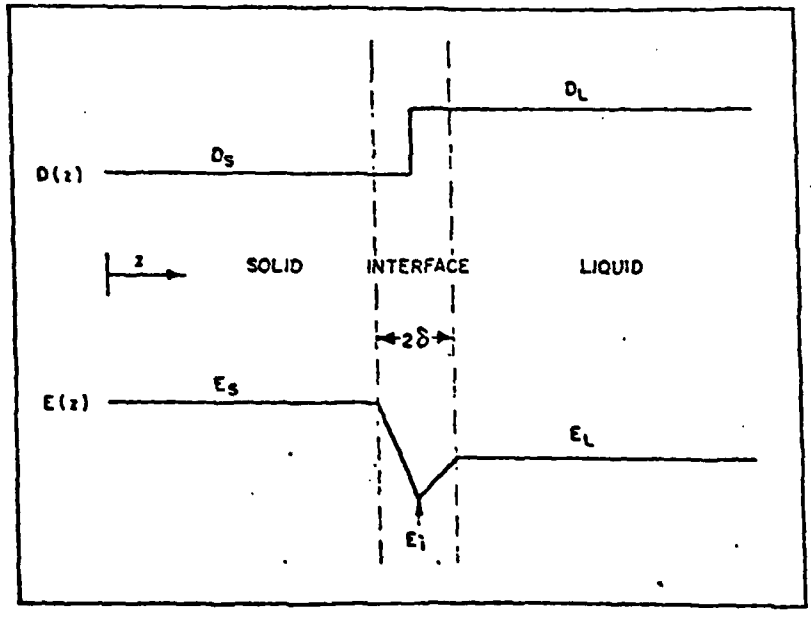

FIGURE 3. Baker's model for solute redistribution allowed for an arbitrarily varying diffusion coefficient and potential energy for solute near the moving interface. The particular form depicted above leads to the redistribution given in equation (3) and depicted in Figure 4.

and solid at the interface leads to the following expression (22).

$$(C_L/C_s)_{int} = \{\exp(-\alpha-\beta) + \exp(-\beta)[k_e/k_i - \exp(-\alpha)]/$$

$$[1 + \ln(k_e/k_i)/\alpha] + k_e[1-\exp(-\beta)/k_i]/[1+\ln k_i/\beta]\}/k_e \quad (3)$$

where

$$k_e = \exp[(E_L-E_s)/kT]$$

$$k_i = \exp[(E_L-E_i)/kT]$$

are the equilibrium segregation coefficients between liquid and solid or interface respectively and

$$\alpha = \delta V/D_s$$

$$\beta = \delta V/D_L$$

are reciprocals of diffusion distances (in units of the boundary thickness δ) in solid and liquid respectiyely. Figure 4 shows the result for $k_e = 0.1$ and $D_s/D_L = 10^{-3}$.

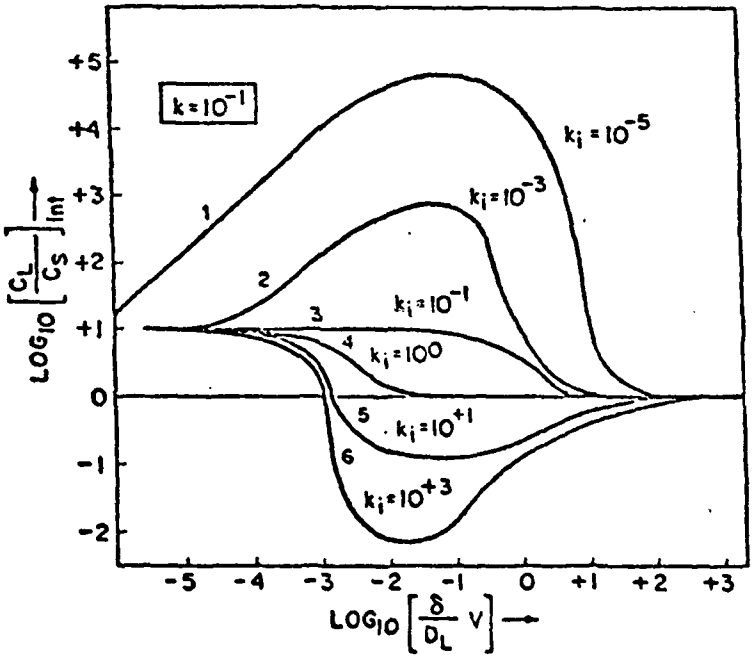

FIGURE 4. Partitioning at interface as a function of imposed growth rate for the model depicted in Figure 5 (from (22).

Let us first examine curves 3 and 4 for which E_i is E_s and E_l respectively. For these special conditions the energy curve in Figure 3 has a single ramp which occurs in a region of liquid or solid diffusion respectively. Comparison of the two shows the effect of shifts of the energy ramp relative to the discontinuity in diffusivity. When the solute is in the energy ramp it experiences a drift force. In curve 4 this drift is exerted when the diffusivity is much lower than it is for the model of curve 3. Trapping occurs at lower velocities. For curves 1 and 2 the solute is first repelled from the interface. Segregation over a wide range of velocities is stronger than equilibrium until at the highest velocities trapping finally occurs. Chernov's ideas are modelled in curves 5 and 6. The solute is attracted to the interface and then buried in the solid. Trapping occurs at quite low velocities, but in the intermediate velocity range segregation to the solid is so strong that the effect overshoots. Baker concluded that Chernov's ideas were not necessary to explain trapping. He also concluded that very accurate modelling of interface structure, kinetics and energetics would be necessary to obtain valid predictions about solute trapping except at the very highest velocities. Curves 3 and 4 are quite similar to the model presented by Jackson, et al. (26) at this conference.

The thermodynamic questions raised by solute trapping were explored extensively by Baker and Cahn (7). Of particular interest is the T_0 curve which is the intersection of the solid and liquid free energy plotted on a phase diagram. It not only marks a bound for diffusionless solidification in which solid and liquid can have the same composition; it also marks the bound on solid compositions which can form from liquid of any composition at that temperature. Where thermodynamic data are accurate enough to predict metastable extensions of free energy functions, T_0 curves can be obtained. For the retrograde systems a simple estimate can be constructed for the maximum composition that the T_0 curve reaches at 0°K. No solid of this phase in excess of this maximum can form from the liquid no matter how rapidly cooled, unless local equilibrium ceases for the liquid phase itself.

This estimate is obtained from a rigorous relationship (27,28) for the slope of the solidus curve.

$$\frac{dT}{dc_s} = -\frac{(c_L - c_s)T(\partial^2 G_s/\partial c_s^2)}{H_L(c_L) - [(1-c_L)\bar{H}_{1s}(c_s) + c_L\bar{H}_{2s}(c_s)]} \qquad (4)$$

where $H_L(c_L)$ is the molar enthalpy of liquid of composition c_L and $\bar{H}_{1s}$ and $\bar{H}_{2s}$ are the partial molar enthalpies of the two components in the solid at composition c_s and G_s is the molar

Gibbs free energy of the solid. At a given temperature the denominator has a simple geometric interpretation on an enthalpy vs. composition plot for the liquid and solid phases (which is relatively independent of temperature). The denominator is the vertical distance at the liquidus composition for that temperature between the liquid enthalpy curve and the tangent drawn to the solid enthalpy curve at the solidus composition. Hence, at the retrograde temperature, where the slope of the solidus is infinite, the denominator is zero and the tangent crosses the liquid enthalpy curve at the liquidus composition (q) in Figure 5. At low temperatures where enthalpy is the dominant term in the free energy, the T_0 composition can be approximated by the intersection of the enthalpy curves. In the absence of any information about the curvature of the solid enthalpy to determine the intersection (p) of the enthalpy curves, an approximate limit on the T_0 composition can be obtained by the intersection of the previously mentioned tangent and the liquid enthalpy curve (q). This intersection is the liquidus composition at the retrograde temperature. The T_0 curve is an absolute limit to solute trapping and its exact location is important for many rapid solidification predictions (31). Such a limit seems to have been observed by

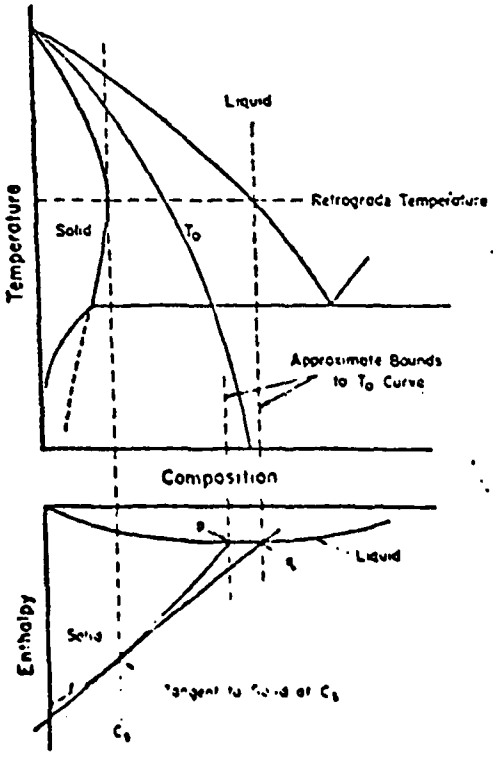

FIGURE 5. Using the rigorous relationship Eq. (4) between solidus slope and enthalpy curves, the liquidus composition at the retrograde can be shown to be the intersection (q). This composition approximates pt. (p) the intersection of the liquid and solid enthalpy curves which is an estimate of the T_0 composition at absolute zero.

White et al. (20). In Table I we give the maximum equilibrium solid solubility at the retrograde c_s^r, the liquid composition at the retrograde c_L^r, or where it isn't known an estimate c_s^r/k_0, and the maximum solid composition that has been observed to date. Except for Si(As), c_s^{max} is less than c_L^r (or c_s^r/k_0), consistent with the estimated thermodynamic bound given above. Every one of these systems shows solute trapping but T_0 is a limit to how far this can be pushed regardless of the solidification rate. These systems are approaching our estimate of this limit. It will be worthwhile to increase solidification rates still further to test the existence of this limit. When calorimetric or free energy data for these systems become available a more precise estimate of the composition at the crossing of the enthalpy curves, which is the rigorous basis of the thermodynamic limit, should be substituted for c_L^r.

ACKNOWLEDGMENTS

This work was partially supported by a contract from the Defense Advanced Research Projects Agency.

Table I. Comparison of the Liquidus Composition at the Retrograde Temperature with the Maximum Solid Solubility Found in Rapid Solidification

Solvent (solute)	c_s^r	c_L^r	c_s^r/k_0	c_s^{max} *Observed*	*Comments*
Zn(Cd)	*0.025*	*.22(29)*		*.10(19)*	*mole fractions*
Si(As)	$1.5x10^{21}$		$5x10^{21}$	$6x10^{21}$ *(20)*	*atoms/cc, k_0 from (30)*
Si(Sb)	$7x10^{19}$		$3x10^{21}$	$1.3x10^{21}$ *(20)*	*atoms/cc, k_0 from (30)*
Si(Ga)	$4.5x10^{19}$		$6x10^{21}$	$4.5x10^{20}$ *(20)*	*atoms/cc, k_0 from (30)*
Si(In)	$8x10^{17}$		$2x10^{21}$	$1x10^{20}$ *(20)*	*atoms/cc, k_0 from (30)*
Si(Bi)	$8x10^{17}$		$1x10^{21}$	$4x10^{20}$ *(20)*	*monotectic*

REFERENCES

1. F. F. Abraham, Homogeneous Nucleation Theory, Academic Press, New York (1974).
2. K. Vonnegut, Cat's Cradle, Delacorte, New York (1971).
3. M. C. Flemings, Solidification Processing, McGraw Hill, New York (1974).
4. J. W. Cahn, W. B. Hillig, G. W. Sears, Acta Met. 12, 1421 (1964).
5. G. J. Abbaschian and S. F. Ravitz, J. Crystal Growth 28, 16 (1975); 44, 453 (1978).
6. W. Bardsley, J. B. Mullin and D.T.J. Hurle, Solidification of Metals, Iron and Steel Inst. Pub. No. 110, London (1968) p. 93.
7. J. C. Baker and J. W. Cahn, Solidification, ASM, Metals Park, Ohio (1971) p. 23.
8. W. A. Tiller, K. A. Jackson, J. W. Rutter and B. Chalmers, Acta Met. 1, 428 (1953).
9. W. W. Mullins and R. F. Serkerka, J. Appl. Phys. 35, 444 (1964).
10. R. F. Sekerka, Crystal Growth: An Introduction, Ed. P. Hartmen, North-Holland, Amsterdam (1973) p. 403.
11. R. T. Delves, Crystal Growth, Vol. 1, Ed. B. R. Pamplin, Pergamon, Oxford (1974) p. 40.
12. D. J. Wollkind, Preparation and Properties of Solid State Materials, Vol. 4, Ed. W. R. Wilcox, Marcel Dekker, New York (1979) p. 111.
13. R. F. Sekerka, Crystal Growth, Ed. H. S. Peiser, Pergamon, Oxford (1967) p. 691.
14. R. F. Sekerka, J. Appl. Phys. 36, 264 (1965).
15. S. R. Coriell and R. F. Sekerka, J. Crystal Growth 34, 157 (1976).
16. J. W. Cahn, Theoretical Aspects of the Formation of Cells and Dendrites, in Japan-U.S. Joint Seminar on Solidification of Metals and Alloys, Jap. Soc. for the Promotion of Science, Tokyo, Japan (1977) p. 1-14.
17. K. A. Jackson, Liquid Metals and Solidification, ASM Cleveland (1958) p. 174.
18. K. A. Jackson, Can. J. Phys. 36, 683 (1958).
19. J. C. Baker and J. W. Cahn, Acta Met. 17, 575 (1969).
20. C. W. White, S. R. Wilson, B. R. Appleton, F. W. Young, Jr., and J. Narayan, these proceedings.
21. H. J. Leamy, J. C. Bean, and T. M. Poate, Solute Trapping During Laser Annealing of Silicon, in press.
22. J. C. Baker, Interfacial Partitioning During Solidification, PhD Thesis, MIT (1970), Chapter V.
23. A. A. Chernov, Growth of Crystals, Vol. 3, Consultants Bureau, New York (1962)., p. 35.

24. J. W. Cahn, Acta Met. 10, 789 (1962).
25. M. Hillert and B. Sundman, Acta Met. 25, 11 (1977).
26. K. A. Jackson, G. H. Gilmer and H. J. Leamy, these proceedings.
27. J. L. Meijering, Philips Res. Rep. 3, 281 (1948).
28. C. Wagner, Thermodynamics of Alloys, Addison Wesley, New York (1952) p. 67.
29. M. Hansen, Constitution of Binary Alloys, McGraw Hill (1958).
30. C. W. White, S. R. Wilson, B. R. Appleton and J. Narayan, these proceedings.
31. T. B. Massalski and Y. Bienvenu, Proc. Sec. Int'l Conf. on Rapidly Quenched Metals, Eds. N. J. Grant and B. C. Giessen, M.I.T., Massachusetts, 2 (1976).